Shock front distortion and Richtmyer-Meshkov-like growth caused by a small pre-shock non-uniformity

A. L. Velikovich,[1] J. G. Wouchuk,[2] C. Huete Ruiz de Lira,[2] N. Metzler,[3] S. Zalesak,[1] and A. J. Schmitt[1]

[1]*Plasma Physics Division, Naval Research Laboratory, Washington, DC 20375, USA*

[2] *Escuela Tecnica Superior de Ingenieros Industriales, Universidad de Castilla-la Mancha, 13071 Ciudad Real, Spain*

[3]*Science Applications International Corporation, McLean, VA 22150, USA, and NRCN, P. O. Box 9001, Beer Sheva, Israel*

Abstract

Response of a shock front to small pre-shock non-uniformities of density, pressure and velocity is studied theoretically and numerically. These pre-shock non-uniformities emulate imperfections of a laser target, due either to its manufacturing, like joints or feeding tubes, or to pre-shock perturbation seeding/growth, as well as density fluctuations in foam targets, "thermal layers" near heated surfaces, etc. Similarly to the shock-wave interaction with a small non-uniformity localized at a material interface, which triggers a classical Richtmyer-Meshkov (RM) instability, interaction of a shock wave with periodic or localized pre-shock perturbations distributed in the volume distorts the shape of the shock front and can cause a RM-type instability growth. Explicit asymptotic formulae describing distortion of the shock front and the rate of RM-type growth are presented. These formulae are favorably compared both to the exact solutions

of the corresponding initial-boundary-value problem and to numerical simulations. It is demonstrated that a small density modulation localized sufficiently close to a flat target surface produces the same perturbation growth as an “equivalent” ripple on the surface of a uniform target, characterized by the same initial areal mass modulation amplitude.

PACS: 52.57.Fg, 52.35.Tc, 47.40.-x, 47.20.-k

I. INTRODUCTION

When an initially symmetric shock wave, perfectly planar or spherical, propagates into a non-uniform medium, its front shape becomes distorted. The perturbed shock front leaves a sonic/entropy/vorticity perturbation field in the shocked fluid behind it. Perturbations produced this way, in turn, can trigger either a Rayleigh-Taylor (RT) or a Richtmyer-Meshkov-like (RM-type)[1] instability growth, particularly if an ablation front or a material interface is present nearby.

The response of shock fronts and post-shock flows to the pre-shock non-uniformities is of interest for a wide range of applications, primarily in the area of laser fusion:

1) In direct-drive laser fusion, one of the most promising methods of suppressing the laser imprint[2] and mitigating the RT growth through tailoring the target adiabat[3] is based on irradiating the target with a short laser pulse (spike) prior to the main pulse that accelerates and implodes it. The spike produces a decelerating shock wave propagating into the target, and a rarefaction wave immediately following it. Such "impulsive loading" of the target has been shown to produce strong oscillations of the shock front and the areal mass in the shocked material, amplifying the non-uniformities due to the target manufacturing imperfections and to the spike pre-pulse imprint.[4, 5] The subsequent strong shock wave produced by the main laser pulse propagates through the perturbation field left after the spike.

2) In some of the direct-drive laser fusion target designs, the ablator is a layer of DT wetted or empty plastic foam[6] that helps increase the driving laser beam absorption in the ablator and improve its stability. Foam, being uniform on the average, contains small-

scale density non-uniformities, which might affect the macroscopic shock dynamics.[7] It is important to know whether or not the small-scale foam non-uniformities can also contribute to the shock and areal mass perturbation growth in the target.

3) There are certain practical advantages of having spherical laser fusion targets manufactured with some localized non-uniformities, such as a "thin annular joint extending from the inner to the outer shell radius," where two beryllium hemispheres are bonded,[8] or "a narrow bore fill tube to charge an ignition capsule *in situ* with deuterium-tritium fuel."[9]

4) Deformation of a blast wave in long thin regions of lower density was first observed during nuclear testing and later labeled "the thermal layer effect,"[10] and extensively studied, see Ref. 11 and references therein. Such pre-shock "thermal layers," where the temperature is higher and the density lower than in the ambient medium, thereby forming a "wall-supported shock precursor," can be produced near heated walls in shock-tube,[12] laser[13] and plasma-focus[14] laboratory experiments.

Small-amplitude theory describing the interaction of a shock wave with a non-uniformity localized at a material interface had been first developed by Richtmyer[15] and later advanced by many researchers, see Refs. 16-17 and references therein. Given the importance of shock interaction with small pre-shock non-uniformities for many applications, it is rather surprising that Richtmyer' approach has not been extended so far to produce a theory describing the shock distortion and the post-shock flow evolution caused by the pre-shock non-uniformities distributed in the volume.

In this article, we present such a theory based on small-amplitude, linear stability analysis, for a planar geometry. The background post-shock and pre-shock fluids are

assumed to be uniform, and the unperturbed shock strength maintained constant in time. The pre-shock perturbations considered are non-propagating structures, such as density/entropy modulation, as well as standing sonic waves. We present the results for a shock wave which is either incident from a half-space where there is no non-uniformity (isolated) or supported by a piston. A free surface and an ablation front, where a constant pressure is maintained, and a rigid wall are examples of the piston considered below. Some of the results of our theory are directly applicable to, and the other are easily generalized for the case when a RM-unstable material interface serves as a piston driving a constant-strength transmitted shock wave into a weakly non-uniform fluid. Our theory applies to the shock interaction with small-amplitude non-uniformities, both periodic and localized in space, such as "joints", "tubes" and "thermal layers." It is not applicable to a blast wave, whose strength decreases with time,[11] or to a shock wave driven up the density gradient produced by a spike.[2-5] Further development of the theory to cover these cases is obviously needed, which is beyond the scope of the present article.

In Section II we present formulation of the problem, perturbation equations, boundary conditions, and the elementary theory of shock distortion for the simplest cases. In Section III we describe the general theory and compare the time evolution of the perturbed shock front to our explicit asymptotic formulae. Section IV compares our analytical results with numerical simulations. In Section V we conclude with a discussion.

II. FORMULATION OF THE PROBLEM AND ELEMENTARY THEORY

A. Perturbation equations, initial and boundary conditions

Consider a planar shock wave incident at $t = 0$ upon a half-space $x \geq 0$. The fluid ahead of the shock front is weakly non-uniform:

$$\begin{aligned} r &= r_1 + dr(x,y,t); \qquad p = p_1 + dp(x,y,t); \\ v_x &= dv_x(x,y,t); \qquad v_y = dv_y(x,y,t); \end{aligned} \tag{1}$$

we suppose that dr / r_1, dp / p_1, dv_x / a_1 and dv_y / a_1 are all much less than unity, where a_1 is the pre-shock speed of sound (indices 1 and 2 refer to pre- and post-shock quantities, respectively). In the zero-order approximation, neglecting the small non-uniformities, we have a planar shock wave propagating at constant velocity *D* into a uniform fluid. The mass velocity of the fluid behind the shock front with respect to the pre-shock fluid is denoted *U*; obviously, the density compression ratio in the shock wave is related to these velocities by

$$R = \frac{r_2}{r_1} = \frac{D}{D-U}. \tag{2}$$

Below we assume ideal gas equation of state of the fluid with adiabatic exponent *g*. The average post-shock values of density, pressure and sound speed are[18]

$$\begin{aligned} r_2 &= \frac{(g+1)M_1^2}{(g-1)M_1^2+2}\, r_1, \qquad p_2 = \frac{2gM_1^2 - g + 1}{g+1}\, p_1, \\ a_2 &= \frac{\sqrt{\left(2gM_1^2 - g + 1\right)\left[(g-1)M_1^2 + 2\right]}}{(g+1)M_1}\, a_1, \end{aligned} \tag{3}$$

where $M_1 = D / a_1 > 1$ is the Mach number of the incident shock. We will use the reference frame in which the shocked fluid is at rest and $x = 0$ corresponds to the position of the planar shock front at $t = 0$. In this reference frame, the shock front

propagates at the velocity $D-U$ with respect to the shocked fluid. The corresponding downstream Mach number is

$$M_2 = \frac{D-U}{a_2} = \sqrt{\frac{(g-1)M_1^2+2}{2gM_1^2-g+1}} < 1. \tag{4}$$

Our small-amplitude analysis is based on Fourier decomposition of all perturbations. We assume their dependence on the transverse coordinate y in the form $\exp(iky)$, where $k \equiv k_y = 2p / l_y$, see Fig. 1(a)-(c). Below k without subscript always means k_y, and the common factor $\exp(iky)$ in perturbation variables is omitted. Let us introduce dimensionless first-order perturbation variables

$$\tilde{r} = \frac{dr}{r_2}, \quad \tilde{p} = \frac{dp}{r_2 a_2^2} = \frac{1}{g}\frac{dp}{p_2}, \quad \tilde{v}_x = \frac{dv_x}{a_2}, \quad \tilde{v}_y = i\frac{dv_y}{a_2}. \tag{5}$$

Then the linearized ideal fluid equations are written as

$$\frac{1}{a_2}\frac{\partial \tilde{r}}{\partial t} + \frac{\partial \tilde{v}_x}{\partial x} + k\tilde{v}_y = 0, \tag{6}$$

$$\frac{1}{a_2}\frac{\partial \tilde{p}}{\partial t} + \frac{\partial \tilde{v}_x}{\partial x} + k\tilde{v}_y = 0, \tag{7}$$

$$\frac{1}{a_2}\frac{\partial \tilde{v}_x}{\partial t} + \frac{\partial \tilde{p}}{\partial x} = 0, \tag{8}$$

$$\frac{1}{a_2}\frac{\partial \tilde{v}_y}{\partial t} - k\tilde{p} = 0. \tag{9}$$

Excluding velocity perturbations from (6)-(9), we obtain the Klein-Gordon equation for the dimensionless pressure perturbation:

$$\frac{1}{a_2^2}\frac{\partial^2 \tilde{p}}{\partial t^2} - \frac{\partial^2 \tilde{p}}{\partial x^2} + k^2\tilde{p} = 0. \tag{10}$$

Equations (6)-(10) must be supplemented by the boundary conditions at the surface of the piston driving the shock and at the shock front. For both the rigid piston and the free surface boundary conditions, the piston is formed by the fluid particles which initially were located at $x = 0$. For the rigid piston the boundary condition at $x = 0$ is

$$\tilde{v}_x = 0; \tag{11}$$

for the free surface, it is

$$\tilde{p} = 0. \tag{12}$$

If the shock wave is driven by a laser, as in laser-fusion-relevant conditions, then the boundary condition should be formulated at the time-dependent position of the ablation front, at $x = v_a t$, where the ablation velocity $v_a = \dot{m} / r_2$, and $\dot{m}$ is the mass ablation rate. The corresponding Mach number is defined as $M_a = v_a / a_2$; in most cases it is small, $M_a << 1$, because the plasma flow near the ablation front is subsonic, almost isobaric. Below we approximate the ablation front with a sharp boundary and use the boundary conditions due to Sanz and Piriz,[19] formulated as in Eqs. (B7) and (9) of Ref. 20:

$$\tilde{p} + \frac{(1-r_D)^2 M_a^2}{r_D} k dx_a + M_a \left[(1-r_D)\tilde{v}_x + \tilde{v}_y\right] + \frac{r_D}{k a_2}\frac{d}{dt}\tilde{v}_x = 0. \tag{13}$$

$$\frac{1}{a_2}\frac{d}{dt} dx_a + M_a k dx_a - \tilde{v}_x = 0. \tag{14}$$

Here, dx_a is the ripple amplitude of the ablation front and $r_D = r_{bl} / r_2$ is the blowoff-plasma-to-ablation front density ratio, which also is typically small, $r_D << 1$. In the limit $M_a \to 0$, $r_D \to 0$, $M_a^2 / r_D \to 0$ Eqs. (13) and (14) are reduced, respectively, to the free-

surface boundary condition (12) and to the conventional relation between the normal velocity and displacement amplitudes at the free surface.

Finally, the "isolated shock" assumption means that the incident shock wave arrives to the $x = 0$ boundary from a half-space filled with a uniform fluid. A weak/contact discontinuity is instantly formed at the fluid particles, where the density modulation begins (which correspond to $x = 0$ in the shocked frame of reference). The perturbations of pressure $\tilde{p}$ and the longitudinal velocity $\tilde{v}_x$ are continuous at $x = 0$, whereas the relative density perturbation $\tilde{r}$ and the *x*-derivative of the lateral velocity, $\tilde{v}_y$, undergo a discontinuity. The flow in the reflected sonic wave is governed by the same equations (6)-(9), which need to be solved additionally to the same equations describing the fluid between $x = 0$ and the shock front because of the discontinuity at $x = 0$. The boundary conditions at the planar front of the reflected sonic wave, at $x = -a_2 t$, are

$$\tilde{v}_x + \tilde{p} = 0, \quad \tilde{v}_y = 0. \tag{15}$$

The boundary conditions at the shock front are perturbed Rankine-Hugoniot (RH) conditions derived in Ref. 18, §90. We write them down here for a particular case of density/entropy pre-shock modulation at constant pressure and zero velocity, characterized by the amplitude $dr_k(x)$, which is supposed to be relatively small at all *x*: $|dr_k(x)|/r_1 << 1$.

$$\tilde{v}_y - M_2(R-1)k dx_s = 0, \tag{16}$$

$$2\tilde{v}_x - \frac{\left(M_1^2+1\right)}{M_1^2 M_2}\tilde{p} = -M_2(R-1)\frac{dr_k}{r_1}, \tag{17}$$

$$\tilde{r} - \frac{1}{M_1^2 M_2^2}\tilde{p} = \frac{dr_k}{r_1}, \tag{18}$$

$$\frac{2}{a_2}\frac{d}{dt}dx_s - \frac{(g+1)}{2M_2}\tilde{p} = -M_2 R\frac{dr_k}{r_1}. \tag{19}$$

Here, dx_s is the displacement amplitude of the shock front, R and M_2 are given by (2)-(4). In the reference frame where the shocked fluid is at rest, the boundary conditions (16)-(19) are imposed at $x_s = (D-U)t = M_2 a_2 t$, which corresponds to $x = Dt$ in the reference frame where the pre-shock fluid is at rest. The initial coordinate-dependent pre-shock density modulation profile $dr_k(x)$ thereby translates into a time-dependent term $dr_k(t)/r_1$ in (17)-(19). Without this term, the boundary conditions (17)-(19) are the same as used by all the researchers who studied propagation of rippled shock waves into a uniform ideal gas, starting from Refs. 21-22. If the pre-shock fluid also contains perturbation of pressure and/or velocity, as, for example, sonic waves (see Section III.D), the corresponding driving terms should be added to the right-hand sides of Eqs. (16)-(19).

Figure 1 demonstrates some examples of pre-shock density modulation profiles studied in this article. The simplest case is periodic lateral variation, independent from the longitudinal coordinate x, "stripes," Fig. 1(a), $dr \propto \cos(k_y y)$, which corresponds to constant values of the density modulation terms in the right-hand sides of the boundary conditions (17)-(19). Periodicity in both lateral and longitudinal directions, a "quilt" of Fig. 1(b), $dr \propto \cos(k_y y)\cos(k_x x)$, corresponds to single-mode oscillations of these terms in (17)-(19) with the frequency $w = k_x D$. Figure 1(c) demonstrates the case where density modulation is periodic in the lateral direction but concentrated near the $x = 0$

surface, $dr \propto \cos(ky)\exp(-qx)$; the corresponding density modulation terms in Eqs. (17)-(19) decay with time as $\exp(-qDt)$. Finally, Figure 1(d) shows a Gaussian density profile $dr \propto \exp(-q^2 y^2)$, emulating a "thermal layer" or a "joint". This localized pre-shock density modulation is not periodic in the lateral direction; hence our single-mode equations (6)-(10), (13)-(19) are not directly applicable to study it. Nevertheless, having solved the perturbation problem for the simplest "stripes" case of Fig. 1(a), we can address the "joint" case of Fig. 1(d) by using Fourier integral, in the same way as done in Refs. 23 for a shock wave driven by, or reflected from, a rigid piston with a Gaussian perturbation.

Figure 2 illustrates the perturbation problem formulation for the "stripes" case of Fig. 1(a) and the shock wave driven by a rigid piston. The shock front moves from the piston in the positive *x* direction. In our reference frame, where the piston is at rest, the unperturbed coordinate of the shock front is $x_s = (D-U)t = M_2 a_2 t$, see above. Deviation of the shock front from its original planar shape is caused by the interplay of the pre-shock non-uniformity of density and the post-shock non-uniformity of all the fluid variables. Our goal is to determine the time dependence of the shock front displacement amplitude, $dx_s(t)$, as well as the dynamics of the other perturbed variables in the shocked fluid.

B. Elementary theory

The problem of shock interaction with pre-shock density perturbation has an elementary asymptotic solution for the simple case of an isolated shock wave coming from the unperturbed fluid. In this case, it is sufficient to calculate the amplitudes of the

perturbations which represent waves radiated downstream with respect to the shock front. The solution is obtained for the general case of a "quilt," Fig. 1(b):

$$\frac{dr_k}{r_1} = e_k \cos(k_x x), \tag{20}$$

where $e_k << 1$ is a dimensionless constant. The "stripes" case of Fig. 1(a) is recovered in the limit $k_x \to 0$.

Assuming that the displacement of and the pressure perturbation at the shock front after some transient period oscillate harmonically at the frequency $w = k_x D$, we can find the amplitudes of these oscillations. To do this, we decompose the perturbation behind the shock front into an outgoing sonic wave, a vortex wave and an entropy wave:

$$\tilde{p} = \tilde{p}^{(s)}, \quad \tilde{v}_x = \tilde{v}_x^{(s)} + \tilde{v}_x^{(v)}, \quad \tilde{v}_y = \tilde{v}_y^{(s)} + \tilde{v}_y^{(v)}, \quad \tilde{r} = \tilde{r}^{(s)} + \tilde{r}^{(e)} \tag{21}$$

where the superscripts *s*, *v* and *e* refer to the sonic, vorticity and entropy perturbations, respectively.

The sonic pressure perturbation $\tilde{p} = \tilde{p}^{(s)}$ satisfies the wave equation (10). We seek a solution of (10) that at $x = M_2 a_2 t$ oscillates at the frequency w in the form

$$\tilde{p}^{(s)} = \tilde{p}_0 \exp[-iwt + kh(x - M_2 a_2 t)], \tag{22}$$

where h is a constant to be determined. Substituting (22) into (10), we obtain the dispersion relation

$$(iw + ka_2 M_2 h)^2 - k^2 a_2^2 h^2 + k^2 a_2^2 = 0, \tag{23}$$

from which we find the parameter h:

$$h_{1,2} = \frac{1}{\sqrt{1 - M_2^2}} \left(\pm \sqrt{1 - z_0^2} + iM_2 z_0 \right), \tag{24}$$

where we have defined

$$z_0 = \frac{k_x R M_2}{k_y \sqrt{1 - M_2^2}}. \tag{25}$$

We see that the sonic perturbations downstream behave differently for the values of the parameter z_0 less and greater than unity. In the former case, the real part of the parameter h is nonzero, which implies that the corresponding pressure perturbations (22) either grow or decay exponentially with the distance from the shock front. Physically, it means that our combination of the frequency $w = k_x D$ and the lateral wavenumber k_y does not correspond to a running sonic wave. The perturbation amplitudes are thereby maintained finite at the shock front by the external driving force (pre-shock density modulation) and decay with the distance from the shock front. The corresponding condition on the ratio of longitudinal and lateral wavenumbers can be re-written as

$$\frac{k_x}{k_y} < \frac{\sqrt{1 - M_2^2}}{R M_2}. \tag{26}$$

If the long-wavelength condition (26) is satisfied, and thereby $z_0 < 1$, then we are interested in the sonic mode that decays with the distance from the shock front, at $x \to -\infty$, that is, one corresponding to the solution (24) with the positive real part

$$h = \frac{1}{\sqrt{1 - M_2^2}} \left(\sqrt{1 - z_0^2} + i M_2 z_0 \right). \tag{27}$$

If (26) is not satisfied, $z_0 > 1$, then both solutions (24) are imaginary, and the pressure perturbations are running sonic waves. The outgoing wave corresponds to

$$h = \frac{i}{\sqrt{1 - M_2^2}} \left(-\sqrt{z_0^2 - 1} + M_2 z_0 \right). \tag{28}$$

Sonic velocity perturbations $\tilde{v}_x^{(s)}$ and $\tilde{v}_y^{(s)}$ are proportional to the same exponential factor (22), and their amplitudes are found from Eqs. (8), (9):

$$\tilde{v}_{x0}^{(s)} = \frac{h\tilde{p}_0}{M_2 h + iz_0\sqrt{1-M_2^2}}, \qquad \tilde{v}_{y0}^{(s)} = -\frac{\tilde{p}_0}{M_2 h + iz_0\sqrt{1-M_2^2}}. \tag{29}$$

Velocity perturbations in the vortex wave are arbitrary functions of x, satisfying the divergence-free condition $\partial\tilde{v}_x^{(v)}/\partial x + k\tilde{v}_y^{(v)} = 0$. At the shock front, $x = M_2 a_2 t$, these functions should oscillate, which determines the coordinate dependence of these velocities. For the longitudinal velocity we have

$$\tilde{v}_x^{(v)} = \tilde{v}_{x0}^{(v)} \exp\left(-i\frac{wx}{M_2 a_2}\right) = \tilde{v}_{x0}^{(v)} \exp\left(-ikx\frac{z_0\sqrt{1-M_2^2}}{M_2}\right). \tag{30}$$

The coordinate dependence is the same for the lateral velocity perturbation, whereas its amplitude $\tilde{v}_{y0}^{(v)}$ is expressed via $\tilde{v}_{x0}^{(v)}$ with the aid of the divergence-free condition:

$$\tilde{v}_{y0}^{(v)} = i\frac{z_0\sqrt{1-M_2^2}}{M_2}\tilde{v}_{x0}^{(v)}. \tag{31}$$

At the shock front $\tilde{p} = \tilde{p}_0$, $\tilde{v}_x = \tilde{v}_{x0}^{(s)} + \tilde{v}_{x0}^{(v)}$, $\tilde{v}_y = \tilde{v}_{y0}^{(s)} + \tilde{v}_{y0}^{(v)}$. The two unknown amplitudes, $\tilde{p}_0$ and $\tilde{v}_{x0}^{(v)}$, and the dimensionless shock ripple amplitude kdx_s are immediately determined from the RH boundary conditions (16), (17) and (19), where we have to substitute $1/(ka_2)(d/dt) = -iz_0\sqrt{1-M_2^2}$.

For the long-wavelength "quilt" case, when (26) is satisfied, the asymptotic expression for the shock ripple amplitude is

$$kdx_s(t) \cong -e_k Q\sqrt{\frac{1-b_1 z_0^2}{1+b_2 z_0^2+b_3 z_0^4}}\cos(k_x Dt - f), \tag{32}$$

where the constants are defined as

$$Q = \frac{RM_2^2}{\sqrt{1-M_2^2}}, \quad b_1 = 1 - \frac{1}{M_1^4 M_2^2},$$
$$b_2 = 2\left(2M_2^2 - 1 - \frac{1}{M_1^2}\right), \quad b_3 = \left(1 + \frac{1}{M_1^2}\right)^2 - 4M_2^2, \tag{33}$$
$$f = \arctan\frac{2M_2 M_1^2 z_0\sqrt{1-z_0^2}}{M_1^2 - (M_1^2+1)z_0^2} - \arctan\frac{z_0}{M_1^2 M_2\sqrt{1-z_0^2}},$$

and the value of $\arctan(...)$ in the definition of f is taken between $p/2$ and p if its argument is negative.

In particular, for the limiting case of "stripes" pre-shock density modulation, $k_x = 0$, hence $z_0 = 0$, and (32) reduces to

$$k dx_s(t) \cong -e_k Q. \tag{34}$$

Physical interpretation of (34) is simple. When a planar shock wave starts propagating along the "stripes" of the density profile shown in Fig. 1(a), initially it moves faster where the density is lower. It happens because the post-shock flow is subsonic, and the pressure there rapidly equilibrates, and the shock velocity scales as $D \propto \sqrt{p/r}$, where p is the post-shock pressure, and r is the pre-shock density. The initially planar shape of the shock front is distorted, becoming convex where the density is lower and concave where it is higher, see Fig. 2, and thereby equilibrating the pressure and reducing the difference in velocities. Eventually the shock approaches a constant velocity and a steady-state rippled shape, the asymptotic shock ripple amplitude being given by (37). Since $Q > 0$, the negative sign in (34) means that the shock is farther from the piston where the pre-shock density is initially lower.

For the "quilts" with very long longitudinal wavelengths, $k_x << k_y$, $z_0 << 1$, Eq. (32) demonstrates that the shock ripple amplitude adjusts to the slowly varying local value of the density modulation amplitude, $e_k \cos(k_x Dt)$. The coefficient of proportionality between the shock ripple amplitude and the pre-shock density modulation amplitude is close to the value $-Q$ characteristic of the "stripes" case (the correction is of the order of z_0^2). There is, however, a phase delay f between the pre-shock density modulation and the shock ripple, so that the former peaks not when the shock passes a valley of density modulation, but slightly later. With increased k_x, the amplitude of oscillations monotonically increases compared to the "stripes" case, by a factor varying from 1 at $z_0 \to 0$ to $1/M_2 > 1$ at $z_0 = 1$. The phase shift f also increases from 0 to $p/2$ at $z_0 = 1$.

For the short-wavelength "quilt," when (26) is not satisfied and $z_0 > 1$, the asymptotic expression for the shock ripple amplitude is

$$k dx_s(t) \cong -e_k Q \frac{z_0 + M_1^2 M_2 \sqrt{z_0^2 - 1}}{M_2 \left[\left(M_1^2 + 1 \right) z_0^2 + 2 M_1^2 M_2 z_0 \sqrt{z_0^2 - 1} - M_1^2 \right]} \sin(k_x Dt). \qquad (35)$$

In this regime, the phase shift between the density modulation and the shock ripple has a constant value of $p/2$, so that the shock ripple amplitude peaks where the pre-shock density modulation has zero value. The asymptotic normalized amplitude (35) of the short-wave shock ripple oscillations decreases with increased longitudinal wavenumber as k_y / k_x, and the limit $k_x / k_y \to \infty$ it can be presented as

$$k_x dx_s(t) \cong -e_k \frac{M_1^2 M_2 + 1}{2 M_1^2 M_2 + M_1^2 + 1} \sin(k_x Dt). \qquad (36)$$

The above formulae have been obtained for the isolated shock boundary condition. However, for the "stripes" and long-wavelength "quilt" cases the outgoing sonic perturbations exponentially decay with the distance from the shock front. Therefore the perturbed shock front in these cases becomes decoupled from the piston at late time, $t \to \infty$. Consequently, the asymptotic formulae (32) and (34) are valid for arbitrary boundary conditions at the piston.

This is not the case for the short-wavelength regime, when the perturbed shock front radiates running sonic waves into the shocked fluid. If the incident shock wave is not isolated but driven by a piston, then these sonic waves, having been reflected from the piston, might reach the shock front again, adding new, Doppler-downshifted frequencies to its oscillations, and thereby making the asymptotic formulae (35) and (36) inapplicable. Extending the above derivation to cover this case is possible but probably too complicated. To study the short-wavelength case in the presence of a piston, we will apply more advanced theoretical methods described in Section III.

Here we limit ourselves to the simplest case of longitudinal density stratification that produces sonic waves propagating from the piston and back. Let us take the lateral wavenumber $k = 0$ and $dr / r_1 = e_0 f(x)$, where $e_0 << 1$ is the small dimensionless amplitude of the pre-shock longitudinal density modulation, and $f(x)$ is an arbitrary function describing its profile. Then Eq. (10) becomes a one-dimensional wave equation, whose general solution is a combination of running waves. We present it in the form

$$\begin{aligned} &\tilde{v}_x = -F(a_2 t + x) + R_p F(a_2 t - x), \quad \tilde{v}_y = 0, \\ &\tilde{p} = F(a_2 t + x) + R_p F(a_2 t - x), \quad \tilde{r} = \tilde{p} + G(x). \end{aligned} \tag{37}$$

Here, R_p is the reflection coefficient for the sonic waves incident upon the piston; $R_p = 1$, -1, and 0 for the rigid piston, free surface and isolated shock boundary conditions, (11), (12), and (15), respectively. Obviously, the solution (37) identically satisfies Eqs. (6)-(10) and the boundary conditions (11), (12) or (15) with arbitrary functions $F(x)$ and $G(x)$. These functions are easily determined if we substitute (37) into (17) and (18). The result is:

$$F(x) = \frac{e_0}{4} M_2 (R-1)(R_s+1) \sum_{n=0}^{\infty} (R_p R_s)^n f\left(\frac{RM_2 x}{1+M_2} \left(\frac{1-M_2}{1+M_2} \right)^n \right), \tag{38}$$

where

$$R_s = \left(\frac{1-M_2}{1+M_2} \right)^2 \frac{2(g-1)M_2 - 3 + g}{2(g-1)M_2 + 3 - g} \tag{39}$$

is the reflection coefficient for the sonic waves normally incident upon the shock front from downstream. Substituting the solution (38) into the boundary condition (18), one can easily determine the entropy perturbation profile $G(x)$. The infinite series (38) describes multiple reverberations of sonic waves between the shock front and the piston; the coefficient $[(1-M_2)/(1+M_2)]^n$ accounts for the Doppler shift of the reverberating wave after *n* reflections from both surfaces. The reflection coefficient R_s varies between zero, for weak shock waves, and some peak value, which for $g \le 5/3$ is achieved for strong shock waves. This peak value is small for typical gammas, varying from –0.0557 for $g = 5/3$ to –0.139 for $g = 7/5$. This is why the series (38) rapidly converge for not-too-small gammas.

To give an example, consider a periodic pre-shock density stratification, $f(x) = e_0 \cos k_x x$. Substituting the solution (37) and (38) into (19), we find the time dependence of the shock displacement amplitude:

$$k_x dx_s(t) = -e_0 \frac{M_1^2 M_2 + 1}{2M_1^2 M_2 + M_1^2 + 1} \sin k_x Dt + e_0 R_p \frac{(1+R_s)^2 (1+M_2)^2}{8M_2^3 R} \sum_{n=1}^{\infty} \left(R_s R_p \frac{1+M_2}{1-M_2} \right)^{n-1} \sin\left(k_x Dt \left(\frac{1-M_2}{1+M_2} \right)^n \right). \quad (40)$$

For the isolated shock case $R_p = 0$ and (40) is reduced to (36), as it should be.

III. SOLUTION BY MEANS OF LAPLACE TRANSFORMS

Here we present general equations describing the temporal evolution of the perturbations in the space filled with the compressed fluid for both situations of long and short wavelength. This can be done, in principle, for arbitrary boundary conditions at the surface $x = 0$. The Laplace transform technique that we use was first developed and applied to the study of perturbed shock evolution by Zaidel in Ref. 22. Here, as had been done in Refs. 16, the idea is to derive exact analytical expressions for the Laplace transform of the shock front pressure perturbations or of the shock front ripple. For the isolated shock case, which represents the simplest of the boundary conditions imposed downstream of the shock surface, we arrive to an exact closed form expression for the Laplace transform of the perturbations. Inverting this Laplace function, we can follow the evolution of almost any quantity of interest in the compressed fluid, always in linear theory. For all other cases, the advantage of using exact expressions for the Laplace transforms of the perturbation variables lies in the possibility of getting accurate information on the asymptotic behavior of the involved functions. The exact solutions

describing the shock distortion and mass flow in this Section I are obtained using either the exact inversion of the Laplace transform, for the isolated shock case, or the Taylor series expansion method (see Ref. 1 and references therein), for all other cases.

A. Pre-shock density modulation periodic in the lateral direction – "stripes"

We start with the simplest of the boundary conditions, that of an isolated shock front. That is, we assume that there is no piston or surface reflecting the sound waves back to the shock front from behind. In general, the shock front will be rippled and the corrugations in its shape will induce a mass flow which is tangential to its surface. This lateral mass flow, in turn, creates a perturbed pressure gradient along it. As a consequence, the shock radiates sonic waves downstream, which are never reflected back to the shock front. This case represents a direct extension of the original Richtmyer's problem (an incident planar shock interacts with an interfacial density non-uniformity[15]) for the case when the non-uniformity is distributed in the volume. In laser-fusion-related applications, the shock is typically driven by a not-too-distant piston. Our isolated shock case serves as a basis for further generalizations that take into account the boundary conditions at the piston, and represents a good approximation in the limit of weak incident shocks for arbitrary boundary conditions at the piston.

For the "stripes" case of Fig. 1(a), $dr_k / r_1 = e_k = \text{const}$, where $e_k << 1$ is the small amplitude of the pre-shock density perturbation $\propto \exp(iky)$. As in Ref. 16, we make a transformation of variables from x and t to r and q, first introduced in the context of a similar problem by Zaidel in Ref. 22 and defined by:

$$r\cosh q = ka_2 t, \quad r\sinh q = kx. \tag{41}$$

The dimensionless shock front coordinate q_s is expressed via the downstream shock Mach number: $\tanh q_s = M_2$. It is convenient to work with the Laplace transform with respect to the variable *r*. We define, for example, the Laplace transform of the shock pressure perturbation amplitude as:

$$\widetilde{P}(s,q_s) \equiv \widetilde{P}_s(s) = \int_0^\infty \widetilde{p}(q_s, r)\exp(-sr)dr, \tag{42}$$

where the variable q_s means that the pressure is evaluated at the shock front position. After some algebra, which can be adapted to this problem following the procedure outlined in Ref. 16, see Appendix, we arrive to an exact solution for the Laplace transform of the pressure perturbations at the shock front (assuming that there are no waves reflected back to the shock front, as also discussed in Ref. 24) in the "stripes" case:

$$\widetilde{P}_s(s) = \frac{(1-a_{10})s^2\widetilde{p}_{s0} + a_{20}}{s\left(s\sqrt{s^2+1} - a_{10}s^2 - a_{11}\right)}. \tag{43}$$

The coefficients a_{10}, a_{11} and a_{20} depend on the fluid equation of state and the shock intensity. The coefficient a_{20} here is different from that defined in Ref. 16, because of the different nature of the perturbations at the shock front. In Ref. 16, the shock ripple amplitude was given as an initial condition at $t = 0^+$, $x = 0$. Here, the shock front ripple is initially zero, and becomes nonzero later on, due to the density modulation in the pre-shock fluid. These coefficients for an ideal gas equation of state (EOS) valid for a more general case of a "quilt" pre-shock density modulation are given by

$$\begin{aligned} a_{10} &= -\frac{(1+M_1^2)}{2M_1^2 M_2}, \quad a_{11} = -\frac{1}{2M_2}, \\ a_{20} &= e_k M_2 \left[\frac{1}{g+1}R - \frac{1}{2}(R-1)z_0^2\right], \end{aligned} \tag{44}$$

and $\widetilde{p}_{s0}$ is the initial pressure perturbation at $t = 0^+$, at the surface $x = 0$:

$$\widetilde{p}_{s0} = \epsilon_k \frac{M_2(R-1)}{2(1-\alpha_{10})}. \tag{45}$$

Here, the downstream Mach number M_2 and the shock compression ratio *R* are given by (4) and (2)-(3), respectively, and z_0 - by (25); in our "stripes" case $z_0 = 0$.

It is also easy to obtain the solution for the Laplace transform of the shock front ripple amplitude kdx_s from the linearized RH equations using our previous results:

$$kdX_s(s) = \left[\epsilon_k \frac{\sqrt{1-M_2^2}}{4M_2^2} + \frac{\alpha_{30}}{s}\left(\sqrt{s^2+1} - \alpha_{10}\right) \right] \times \frac{1}{s\sqrt{s^2+1} - \alpha_{10}s^2 - \alpha_{11}}, \tag{46}$$

where the coefficient α_{30} is defined as

$$\alpha_{30} = -\frac{\epsilon_k R M_2}{2\sqrt{1-M_2^2}}. \tag{47}$$

From Eqs. (43) and (46) we can obtain the temporal evolution of the corresponding perturbations. A conventional way of doing this[22] is to expand the functions given by Eqs. (43) and (46) as a series in the variable $\exp\left(-\sinh^{-1} s\right)$. This decomposition for the Laplace transform, gives rise to an infinite series of Bessel functions in the time domain.[16,17,24] However, we prefer to show here a different approach, that of explicitly inverting the Laplace functions $\widetilde{P}_s(s)$ and $kdX_s(s)$ in the complex plane. This method, albeit apparently more complicated, provides us with an integral representation of the front perturbations, which will be useful for many other purposes, as for example the estimation of the late-time asymptotic behavior.

From the theory of the Laplace transform, we can get the original functions in the time domain, after evaluating an integral of the form:

$$\widetilde{p}(q_s, r) = \int_{c-i\infty}^{c+i\infty} \widetilde{P}_s(s)\exp(sr)ds, \tag{48}$$

where c is a real number to the right of all the singularities of $\widetilde{P}_s$. For ideal gases, as is the case in this work, the right-hand sides of Eqs. (43) and (46) do not have real or imaginary poles except $s = 0$. The other singularities are the branch points at $s = \pm i$, see Ref. 24. After closing the integration contour to the left, and defining a branch cut along the imaginary axis between the branch points $s = +i$ and $s = -i$, we get the following integral representation for the pressure perturbation amplitude at the shock as a function of time:

$$\widetilde{p}_s(t) = \frac{e_k}{p} M_2 (R-1) \int_0^1 \cos(r_s z) z^2 f_p(z) dz + \frac{2a_{20}}{p} \int_0^1 \left(1 - \cos(r_s z)\right) f_p(z) dz, \tag{49}$$

where the time variable r_s is found from (41) at $x = M_2 a_2 t$

$$r_s = \frac{kDt\sqrt{1-M_2^2}}{RM_2}, \tag{50}$$

and the function $f_p(z)$ in (49) is given by

$$f_p(z) = \frac{\sqrt{1-z^2}}{z^2\left(1-z^2\right) + \left(a_{10}z^2 - a_{11}\right)^2}. \tag{51}$$

If we had imposed different boundary conditions behind the shock, other than the isolated shock condition studied in this Section, we would have obtained another auxiliary function $f_p(z)$ inside the integral, in Eq. (49). For example, for rigid piston boundary conditions, or free surface conditions at $x = 0$, the function f_p would be the solution of an inhomogeneous functional equation, which has to be solved with techniques similar to those outlined in Ref. 16, see Appendix.

The Laplace functions obtained before are a very powerful tool. Indeed, it is not difficult to arrive to the late time asymptotic for the pressure perturbations at the shock front. For (49) and (51) we obtain:[24]

$$\widetilde{p}_s(t) \cong \widetilde{p}_s^{\infty} + s_{\,s}\,\frac{\cos r_s - \sin r_s}{r_s^{3/2}} + O\left(r_s^{-5/2}\right), \tag{52}$$

where the quantity $s_{\,s}$ is defined as

$$s_{\,s} = -\frac{e_k}{\sqrt{p}}\left(\frac{M_2(R-1)}{2(1-a_{10})^2} + 8M_1^4 M_2^2\sqrt{\frac{M_1^2-1}{g+1}}\right), \tag{53}$$

and the constant asymptotic pressure perturbation is

$$\widetilde{p}_s^{\infty} = e_k\,\frac{2RM_2^2}{g+1}. \tag{54}$$

Operating in a similar way with the Laplace function of the shock front ripples (46), we get the exact temporal evolution:

$$k dx_s(t) = \frac{e_k(g+1)}{4pM_2\sqrt{1-M_2^2}}\int_0^1\left[M_2(R-1)z - \frac{2a_{20}}{z}\right]\sin\left(r_s z\right) f_p(z)\,dz, \tag{55}$$

where $r_s(t)$ and $f_p(z)$ are defined by (50) and (51), respectively. At $t \to \infty$ we find from (55) that kdx_s approaches the asymptotic value given by (34), as it should be. It is clear that the late time asymptotic of the shock ripple would also show oscillations with an amplitude that decays as $t^{-3/2}$, superimposed upon the constant value given by (34). As noted before, the asymptotic amplitude of the shock front corrugation has opposite sign with respect to that of the pressure disturbance at the same position on the shock surface.

Figure 3 shows the results of the solution for a strong shock with $M_1 = 10$ in an ideal gas with g = 5/3 interacting with the "stripes" pre-shock density modulation. The

dimensionless shock ripple amplitude kdx_s in Fig. 3 is normalized with respect to the dimensionless density variation amplitude, $e_k = dr_k / r_1$, so that its asymptotic value, according to (34), is equal to $-Q$. This value corresponds to the straight horizontal line. Its negative sign means that asymptotically the shock front is farther from the piston where the pre-shock density is initially lower, as shown in Fig. 2. Figure 3 shows the normalized dimensionless shock ripple amplitude vs. the normalized time kDt. It demonstrates that although the time history of the shock ripple amplitude depends on the boundary condition at the piston surface, its constant asymptotic value does not, as predicted by Eq. (34). This example also demonstrates that the shape of a strong shock wave propagating along the "stripes" reaches its asymptotic value after it travels slightly more than one lateral wavelength. For the weak shocks, one wavelength is enough. On the other hand, the oscillations of kdx_s around its asymptotic value (24) decay slowly, cf. (52), decreasing to the ~10% level as the strong shock propagates ~16 wavelengths. This slow decay of oscillations is probably a feature of the ideal-gas equation of state used here, cf. Ref. 25, and particularly Fig. 1 there.

B. Pre-shock density modulation localized in the lateral direction – "joint" and "tube"

It is of practical interest to calculate the response of a shock-piston flow to a spatially localized, rather than periodic, pre-shock density perturbation. An important particular case is a density perturbation concentrated in a planar layer, perpendicular to the shock front, Fig. 1(d), which emulates a "joint" in a laser target[8] or a "thermal layer" near a heated wall.[10-14] Assuming a cylindrical, rather than planar, symmetry of the density perturbation shown in Fig. 1(d), we obtain the case of a "tube," a density

perturbation concentrated in a cylinder perpendicular to the shock front, which emulates a fill tube in a laser target.[9]

To solve this problem, we decompose the pre-shock density perturbation into Fourier integral. For each of the Fourier modes, the problem is reduced to the "stripes" case of Fig. 1(a), which has already been solved above. We only need to substitute this solution into the Fourier integral and to perform the integration.

We start with a simpler "tube" case and limit ourselves to a Gaussian pre-shock density profile, which is decomposed into a Fourier integral as

$$\frac{dr(x,y,z)}{r_1} = e_q \exp\left(-q^2 r^2\right) = \frac{e_q}{4pq^2}\int_0^\infty kdk \exp\left(-\frac{k^2}{4q^2}\right)\int_0^{2p} dq \cos(kr\cos q) \\ = \frac{e_q}{2q^2}\int_0^\infty kdk \exp\left(-\frac{k^2}{4q^2}\right) J_0(kr), \tag{56}$$

where $1/q$ is the characteristic diameter of the pre-shock density perturbation and $e_q << 1$ is its small dimensionless amplitude. The expression under the integral over k is the Fourier amplitude dr_k / r_1 of the planar periodic density perturbation mode corresponding to the wavenumber k. For each of these modes, the solution is given by

$$kdx_{s,k}(t) = \frac{dr_k}{r_1}\Phi(kDt), \tag{57}$$

where $t = kDt$ is the dimensionless time for the k-th mode, $\Phi(t)$ is a known function, the same for all modes (its typical graphs are shown in Fig. 3). Since the shock front is initially planar, $\Phi(0) = 0$; the limit of this function at large argument is given by (34). Therefore, at any time the shape of the perturbed shock front is given by

$$qdx_s(r,t) = \frac{e_q}{2q}\int_0^\infty dk \exp\left(-\frac{k^2}{4q^2}\right) J_0(kr)\Phi(kDt). \tag{58}$$

For large t, the argument of Φ in (58) is large everywhere except at $k = 0$, and we can approximate this function in the Fourier integral by $-Q$, its asymptotic value at large argument, see (34). Then, performing integration over k, we find the time-independent asymptotic shape of the shock front for the "tube" case:

$$qdx_s(r, t \to \infty) \cong -e_q \frac{\sqrt{p}}{2} Q \exp\left(-\frac{1}{2} q^2 r^2\right) I_0\left(\frac{1}{2} q^2 r^2\right), \tag{59}$$

where $I_0(z)$ is the modified Bessel function. The asymptotic shock displacement profile near the axis of the "tube" and far from it therefore is

$$qdx_s(r, t \to \infty) \cong \begin{cases} -e_q \dfrac{\sqrt{p}}{2} Q\left(1 - \dfrac{q^2 r^2}{2}\right), & qr << 1; \\ -e_q \dfrac{Q}{qr}, & qr >> 1. \end{cases} . \tag{60}$$

The asymptotic curvature of the shock front at the axis is

$$\frac{1}{R(t)} = \frac{\partial^2}{\partial r^2} dx_s(r, t)\bigg|_{r=0} \to \frac{1}{R_\infty} = e_q \frac{\sqrt{p}}{2} qQ . \tag{61}$$

Figures 4(a) and 4(b) demonstrate how these asymptotic values, (60) and (61), respectively, are approached at $r = 0$. The dimensionless shock ripple amplitude $qdx_s(r = 0, t)$ and dimensionless curvature $1/qR$ are normalized with respect to e_q, and plotted versus normalized time qDt. We see that the distortion of the shock front caused by the "tube" kind of the pre-shock density perturbation always remains finite, localized in the vicinity of the "tube," at the distance of the order of its diameter, in qualitative agreement with the numerical results of Ref. 9.

For the planar, rather than cylindrical, symmetry of the localized pre-shock density perturbation, the "joint" case, the Fourier integral is written as

$$\frac{dr(x,y)}{r_1} = e_q \exp\left(-q^2 y^2\right) = \frac{e_q}{q\sqrt{p}_q} \int_0^\infty dk \exp\left(-\frac{k^2}{4q^2}\right) \cos ky \,, \tag{62}$$

where, as above, $1/q$ is the characteristic width of the pre-shock density perturbation and $e_q << 1$ is its small dimensionless amplitude. Therefore the shape of the shock front is given by

$$qdx_s(y,t) = \frac{e_q}{\sqrt{p}} \int_0^\infty \frac{dk}{k} \exp\left(-\frac{k^2}{4q^2}\right) \Phi(kDt) \cos ky \,. \tag{63}$$

The asymptotic estimate for this "joint" case cannot be made similarly to (58) because Fourier integral (63) diverges at its lower limit $k = 0$ if $\Phi(kDt)$ is simply replaced by its constant asymptotic value $-Q$. The reason for this divergence is simple. As seen from (34) and (57), the asymptotic shock displacement amplitude is large for long wavelengths (small *k*). In the above "tube" case, the long-wavelength modes occupy a small portion of the phase space, which is why their contribution to the Fourier integral is small. In contrast with this, for a "joint' case the long-wavelength modes make the dominant contribution to the Fourier integral (63), making it diverge at $t \to \infty$. A simple calculation yields the time-dependent asymptotic shape of the shock front for the "joint" case:

$$qdx_s(y, t \to \infty) \cong -e_q \frac{Q}{\sqrt{p}} \left[\ln(qDt) + \Delta - q^2 y^2 \, {}_2F_2\left(1,1;\frac{3}{2},2;-q^2 y^2\right)\right], \tag{64}$$

where ${}_2F_2(a,b;c,d;z)$ is the generalized hypergeometric function,

$$\Delta = \ln 2 - \frac{g_E}{2} + \lim_{t\to\infty}\left[\int_0^t \frac{\Phi(t')}{(-Q)} \frac{dt'}{t'} - \ln t\right], \tag{65}$$

and $g_E = 0.5772...$ is the Euler's constant.

The asymptotic shock displacement profile near the symmetry plane of the "joint" and far from it therefore is

$$qdx_s(y,t\to\infty)\cong\begin{cases}-e_q\dfrac{Q}{\sqrt{p}}\left[\ln(qDt)+\Delta-q^2y^2\right], & |qy|<<1;\\ -e_q\dfrac{Q}{\sqrt{p}}\left[\ln\left(\dfrac{Dt}{|y|}\right)+\Delta\right], & |qy|>>1.\end{cases} \tag{66}$$

The asymptotic curvature of the shock front at the "joint" symmetry plane is

$$\frac{1}{R(t)}=\frac{\partial^2}{\partial y^2}dx_s(y,t)\bigg|_{y=0}\to\frac{1}{R_\infty}=\frac{2e_q}{\sqrt{p}}qQ\,. \tag{67}$$

Equations (66) and (67) predict that the shock perturbation exhibits two spatial scales, in qualitative agreement with the simulation results[11] and the experimental findings.[12, 13] In the vicinity of the "joint" plane its shape retains the characteristic length scale $1/q$; in particular, the radius of its curvature approaches a steady-state value of this order, which is independent from the boundary condition at the piston, similarly to the "tube" case. On the other hand, Eq. (66) predicts unlimited, albeit slow, logarithmic growth of the shock displacement amplitude. It contains the term Δ that depends on the time history of the shock displacement amplitude, and therefore, depends on the boundary conditions at the piston. Note that the asymptotic shape of the shock profile (66) at late times, $qDt>>1$, at large distances from the "joint", $|qy|>>1$, is self-similar, depending on y and t only via the dimensionless combination $Dt/|y|$ and independent of q. Figures 5(a), (b) demonstrate that this is indeed the case. The perturbed shock dynamics is different for the cases of rigid piston (a) and free surface (b) because the parameter Δ equals -0.757 in the former case and 1.71 in the latter. The growth rates, however, approach the same limit for both cases.

C. Double-periodic pre-shock density modulation – "quilt"

Now consider the "quilt" case of double-periodic pre-shock density/entropy perturbation, Fig. 1(b), for the isolated shock case. By proceeding much in the same way as in Section III.A, we get the following exact, closed form expressions for the Laplace transforms. Generalization of (43) and (46) for $z_0 > 0$ gives, respectively,

$$\widetilde{P}_s(s) = s\frac{(1-a_{10})\left(s^2+z_0^{\,2}\right)\widetilde{p}_{s0}+a_{20}}{\left(s^2+z_0^{\,2}\right)\left(s\sqrt{s^2+1}-a_{10}s^2-a_{11}\right)}, \tag{68}$$

$$kdX_s(s) = \left[e_k\frac{\sqrt{1-M_2^2}}{4M_2^2}+\frac{\sqrt{s^2+1}-a_{10}s}{s^2+z_0^{\,2}}\left(\frac{(g+1)a_{20}}{4M_2\sqrt{1-M_2^2}}+a_{30}\left(s-a_{11}\right)\right)\right] \times\frac{1}{s\sqrt{s^2+1}-a_{10}s^2-a_{11}} \tag{69}$$

The time evolution of the pressure and shock ripple perturbations can also be easily obtained, as a function of the shock intensity, fluid compressibility and the parameter z_0. In both Eqs. (68) and (69) we recognize the denominator $s^2+z_0^{\,2}$, whose poles at $s=\pm iz_0$ give rise to oscillations of constant amplitude in the domain of the variable r_s, the frequency of which is z_0. This oscillation is convoluted with another oscillating function. We get, for example, for the shock front ripple:

$$kdx_s(t) = \int_0^1\left[x\sin(r_s z)+g(r_s,z)\right]zf_p(z)dz - e_k\frac{M_2R\sin\left(z_0r_s\right)}{2z_0}, \tag{70}$$

where the auxiliary function $g(r_s,z)$ inside the integral (70) and the coefficient x are given by:

$$g(r_s,z) = \frac{(g+1)a_{20}}{2pM_2\sqrt{1-M_2^2}}\frac{z\sin\left(r_sz_0\right)-z_0\sin\left(r_sz\right)}{z_0\left(z^2-z_0^{\,2}\right)}, \tag{71}$$

$$x = \frac{e_k\sqrt{1-M_2^2}}{pM_2^2}, \tag{72}$$

and $f_p(z)$ is defined by (51). To get an approximate analytical formula valid when the shock is far enough from the surface $x = 0$, we must distinguish the two regimes: long-wavelength $z_0 < 1$ and short-wavelength $z_0 > 1$, as defined in Section II.

For the long-wavelength regime, the pressure perturbation at late time is given by the asymptotic formula

$$\widetilde{p}_s(t) \cong b_{01}\cos(k_x Dt) + b_{02}\sin(k_x Dt), \tag{73}$$

where the coefficients b_{01} and b_{02} are given by:

$$\begin{aligned} b_{01} &= \frac{a_{20}(a_{10}z_0^2 - a_{11})}{z_0^2(1-z_0^2) + (a_{10}z_0^2 - a_{11})^2}, \\ b_{02} &= \frac{a_{20}z_0\sqrt{1-z_0^2}}{z_0^2(1-z_0^2) + (a_{10}z_0^2 - a_{11})^2}. \end{aligned} \tag{74}$$

For the shock front ripple amplitude we reproduce the asymptotic formula (32).

Increasing the longitudinal wavenumber further, we enter the short-wavelength regime, where $z_0 > 1$. The asymptotic formula for the shock pressure perturbation amplitude becomes:

$$\widetilde{p}_s(t) \cong e_0\cos(k_x Dt), \tag{75}$$

with

$$e_0 = -\frac{a_{20}}{z_0\sqrt{z_0^2 - 1} - a_{10}z_0^2 + a_{11}}. \tag{76}$$

The asymptotic formula for the shock ripple amplitude is (35).

The long-wavelength condition (26) for the same parameters as in Fig. 3, $M_1 = 10$, $g = 5/3$, requires $k_x/k_y < 0.5049$. Choosing the wavelength ratio in this range, $k_x/k_y = 1/5$, we expect the asymptotic expression (32) to be valid. Figure 6

demonstrates that this is indeed the case, for the rigid piston and free surface boundary conditions as well as for the isolated shock. As in Fig. 3, the time history of the shock ripple amplitude depends on the boundary condition at the piston, whereas its asymptotic behavior does not.

Figure 7(a) illustrates the short-wavelength "quilt" pre-shock density modulation with $k_x / k_y = 1$, the other parameters being the same as above, for isolated shock case. We see that the asymptotic amplitude and phase predicted by (35) are achieved very rapidly.

This asymptotic expression, however, is not applicable in the presence of a piston driving the shock wave into the short-wavelength "quilt". In this case, not covered by the elementary theory of Section II.B, sonic waves reflected from the piston can reach the shock wave and affect its behavior. The appropriate asymptotic formulae can still be obtained using the Laplace transform technique. Here we present the results, whose derivation is outlined in the Appendix.

For the short wavelength regime with sufficiently large z_0 the sonic waves radiated by the shock at the normalized frequency z_0 given by (25) that corresponds to the physical frequency $w = k_x D$ can be reflected from the piston surface and catch the shock front from behind. This will occur if the *x*-velocity of the reflected sonic wave is greater than the shock speed in the reference frame of the shocked fluid. That is, the angle j that the sonic ray forms with the *x*-axis (normal to the piston surface) must satisfy $\cos j > M_2$, see Ref. 18. This condition can be expressed as

$$z_0 > \cosh 2q_s = \frac{1+M_2^2}{1-M_2^2}. \tag{77}$$

Let us define the auxiliary quantity s_0 by $z_0 = \cosh s_0$. Equation (77) is obviously equivalent to $s_0 > 2q_s$, which is also seen to be the requirement for a "successful reflection at the piston boundary". When this condition is met, the shock starts to oscillate with another normalized frequency z_2 given by:

$$z_2 = \cosh(s_0 - 2q_s). \tag{78}$$

The higher-order terms appear as follows. If the sonic waves emitted at the frequency z_2 could reach the shock surface from behind, after being reflected at the piston, another mode (with a lower frequency z_4) would be excited at the shock front. For this to happen, a requirement similar to Eq. (77) has to be satisfied, which is obtained by replacing $2q_s$ with $4q_s$, $6q_s$, …, etc., in the right-hand side of Eq. (77). The corresponding normalized oscillation frequencies therefore are

$$z_{2n} = \cosh(s_0 - 2nq_s)\ . \tag{79}$$

The number of additional oscillatory modes is thereby finite and equal to

$$N = \left[\frac{\ln\left(z_0 + \sqrt{z_0^2 - 1}\right)}{\ln \dfrac{1+M_2}{1-M_2}} \right], \tag{80}$$

where [z] denotes the largest integer $\le z$.

The reason for the finitude of the spectrum lies in the fact that, once the sonic wave with frequency z_m arrives back to the shock, its reflected wave will be Doppler downshifted in the reference frame of the shocked fluid (with a normalized frequency $z_{m+1} < z_m$). Then, after a finite number of reflections, the frequency of the last excited mode would be eventually so low that the x-velocity of the associated sonic ray is less

than the shock speed with respect to the shocked fluid, $a_2 M_2$, and then the process of "successful reflection" terminates. This phenomenon is totally equivalent to the problem of spontaneous acoustic emission (SAE) for a shock moving into a certain non-ideal gas, in the presence of a reflecting boundary from behind, as discussed in Ref. 24. The difference with the problem being studied here is that in our case, the shock is forced to oscillate because of the pre-shock density modulation, so that the oscillations take place for arbitrary EOS, including ideal gas. In Ref. 24, on the contrary, the initial oscillation was provided by the SAE phenomenon, due to the non-ideal EOS of the fluid into which the shock was moving. The interesting point to note is that, once we make the shock to oscillate with any initial frequency (asymptotically in time, independently of the reason of that oscillation), all the other additional modes that are also seen to be excited at its surface, are just due to this process of successful reflection downstream, and their origin is therefore essentially kinematic.

The asymptotic pressure perturbation and shock front ripple amplitudes are expressed as

$$\widetilde{p}_s(t) \cong \sum_{n=0}^{N} e_{2n} R_p^n \cos\left(\frac{\mathbf{z}_{2n}}{\mathbf{z}_0} k_x D t \right), \tag{81}$$

$$k dx_s(t) \cong \sum_{n=0}^{N} j_{2n} R_p^n \sin\left(\frac{\mathbf{z}_{2n}}{\mathbf{z}_0} k_x D t \right). \tag{82}$$

Here R_p, as above, is the reflection coefficient for the sonic waves incident upon the piston. As in (38) and (40), this factor accounts for the phase and amplitude change of the sonic wave at reflection from the piston. The coefficient e_0 is given by (76); the other coefficients are

$$
\begin{aligned}
&e_2 = \frac{2e_0 z_2 \sqrt{z_2^2 - 1}}{z_2 \sqrt{z_2^2 - 1} - a_{10} z_2^2 + a_{11}};\\
&e_{2n} = \frac{2e_0 z_{2n} \sqrt{z_{2n}^2 - 1}}{z_{2n} \sqrt{z_{2n}^2 - 1} - a_{10} z_{2n}^2 + a_{11}} \prod_{m=1}^{n-1} \frac{z_{2m} \sqrt{z_{2m}^2 - 1} + a_{10} z_{2m}^2 - a_{11}}{z_{2m} \sqrt{z_{2m}^2 - 1} - a_{10} z_{2m}^2 + a_{11}},\\
&2 \le n \le N;
\end{aligned}
\tag{83}
$$

$$
\begin{aligned}
&j_0 = \frac{g+1}{4M_2 \sqrt{1 - M_2^2}} \frac{e_0}{z_0} + \frac{a_{30}}{z_0};\\
&j_{2n} = \frac{g+1}{4M_2 \sqrt{1 - M_2^2}} \frac{e_{2n}}{z_{2n}}, \quad 1 \le n \le N;
\end{aligned}
\tag{84}
$$

The value of j_0 given by (84) is, of course, the same as the coefficient at $\sin(k_x Dt)$ in (35). For the isolated shock case $R_p \to 0$ and (81) and (82) are reduced to (75) and (35), respectively. Otherwise the terms in the sums (81), (82) decrease with increased *n* very rapidly because the reflection coefficient of the sonic waves from the shock front is lower for oblique incidence than for normal incidence (39), and for each higher-order wave returning to the shock front from the piston the angle of incidence is more oblique than for the previous one. Therefore in most cases the two first terms in the sums (81), (82) provide sufficient accuracy. In the limit $k_x / k_y \to \infty$, $z_0 \to \infty$ we have

$z_{2n} / z_0 \to [(1 - M_2)/(1 + M_2)]^n$, and (82) is reduced to (40), as it should be.

When a piston driving the shock wave is present, the lower-frequency oscillations superimposed upon the oscillations at the driving frequency $w = k_x D$ are clearly seen in Fig. 7(b). The asymptotic formula (82) is shown to provide good accuracy with just one extra term, corresponding to $n = 1$, retained.

D. Pre-shock standing sonic wave

All the above results refer to the density modulation ahead of the shock, which, at constant pre-shock pressure, corresponds to an "entropy wave" that is stationary with respect to the resting fluid ahead of the incident shock front. In general, a small perturbation of a uniform resting fluid is decomposed into a density/entropy perturbation, a vorticity perturbation and a sound wave.[18] Our theory can be easily modified for the case when the perturbation ahead of the shock front is either a standing sonic wave or a periodic vortex system. We consider here the former case as an example.

We limit ourselves to the situation when the wave vectors in the two superimposed running sonic waves that make a standing wave are parallel to the shock front, in the *y* direction. (This is because there is no reflection of the incident sonic waves from a shock front, so we cannot form any other standing waves.) Using the above terms, the perturbation pattern at any instant looks like "stripes", Fig. 1(a). The areas of high and low density, however, change places periodically, which is why the shock front feels this upstream perturbation as a "quilt", Fig. 1(b), with pre-shock density and other variables oscillating at $y = 0$. For a given lateral wavenumber k, the frequency of these pre-shock oscillations is $w_1 = ka_1$, where a_1 is the pre-shock speed of sound, see Fig. 2. The perturbations coming to the shock front at the time *t* are

$$\begin{aligned} &dr_k(t) = e_k r_1 \cos(w_1 t), \quad dp_k(t) = e_k p_1 \cos(w_1 t), \\ &dv_{x,k}(t) = 0, \quad dv_{y,k}(t) = -ie_k a_1 \sin(w_1 t), \end{aligned} \tag{85}$$

where the dimensionless amplitude of the sonic wave is $e_k << 1$. The density perturbation (85) is similar to that in a "quilt," Fig. 1(b), with the effective longitudinal wavenumber

$$k_{x,eff} = \frac{k_y}{M_1}. \tag{86}$$

The perturbations of the pressure and lateral velocity are not present in the "quilt." To account for these, the boundary conditions (16)-(19) need to be modified appropriately.

Obviously, for a sufficiently strong shock wave, the ratio $k_{x,eff}/k_y$ becomes small enough to satisfy (26), and we approach the long-wavelength "quilt" case. Physically, the post-shock speed of sound is proportional to the shock velocity, and the pre-shock oscillation frequency $w_1 = ka_1$ for sufficiently strong shocks is much smaller than the corresponding post-shock frequency $w = ka_2$. The resulting requirement on the shock strength is

$$M_1 > \left[\left(\frac{g+1}{g-1}\right)^{1/2} + 1\right]^{1/2}. \tag{87}$$

When the shock wave is sufficiently strong the similarity between the cases of the upstream standing sonic wave and the "quilt" increases approaching equivalence. This is because both velocity and pressure behind the strong shock wave are so much higher than their pre-shock values, that the pre-shock perturbations of these variables can be neglected. On the other hand, density variation in the shock wave is limited, hence the perturbed strong shock wave mostly reacts to the pre-shock density perturbations.

Figure 8 shows the time histories of shock ripple amplitude for $g = 5/3$ and two Mach numbers, $M_1 = 10$ and 25. For $g = 5/3$ Eq. (87) gives $M_1 > \sqrt{3} = 1.732$, hence both of these cases satisfy the long-wavelength condition. The agreement with (32) is good, as it should be.

E. Richtmyer-Meshkov-like instability and lateral mass redistribution

1. RM-type perturbation growth at the inner interface and free surface

It has been demonstrated in Ref. 1 that a fast application of an external pressure to a rippled surface produces a fingering instability similar to the classical RM instability, RM-type instability. We show here that such instability develops even if the loaded surface or interface is initially planar. If the half-space behind the surface $x = 0$ contains pre-shock non-uniformities, then the perturbations needed to drive the instability are instantly deposited at this surface, when a planar shock wave either reaches this surface (isolated shock case) or is launched from it (all other cases involving a non-rigid piston) and brought to the surface by sonic waves.

After $t = 0^+$, the free surface $x = 0$ becomes a vortex sheet, which exhibits a linear ripple growth as in the Richtmyer-Meshkov instability.[1] In the case of isolated shock wave, this surface becomes a small-amplitude weak/contact discontinuity separating two regions of fluid: to the left, $x < 0$, we would have irrotational velocity field generated by the left-facing sonic waves radiated by the rippled shock front since $t = 0^+$. To the right, at $0 < x < M_2 a_2 t$ in the frame of reference of the shocked mass, the fluid is filled with sonic waves plus vorticity and entropy perturbations generated at the shock front.[18] We show here that this interface exhibits a RM-type linear growth, too.

The Laplace transform technique makes it possible to find the asymptotic behavior of the $x = 0$ surface for these cases. For the "stripes" and long-wavelength "quilt" cases of pre-shock density modulation, the velocity perturbation amplitude at the surface $x = 0$ tends to a constant asymptotic value

$$v_{xi}^{\infty} = \tilde{v}_{xi}^{0+} - [\cosh q_s + a_1(q_s)]\tilde{P}_s(q_s) - \frac{a_{20}}{\sinh^2(q_s) + z_0^2}, \tag{88}$$

where the velocity perturbation at $t = 0^+$ is given by $\widetilde{v}_{xi}^{0+} = -M_2(R-1)/2$, see (17). For the isolated shock case the function $\widetilde{P}_s(q)$ defined by (42) is explicitly determined by (43) or (68). The procedure of calculating its value for the free surface case is outlined in the Appendix, where the function $a_1(q_s)$ is defined by Eq. (A3).

For the short-wavelength "quilt", sonic waves radiated downstream by the rippled shock front reach the $x = 0$ surface and make it oscillate. The number of the oscillating modes is

$$N' = \left[\frac{\ln\left(z_0 + \sqrt{z_0^2 - 1}\right)}{\ln \dfrac{1+M_2}{1-M_2}} + \frac{1}{2} \right], \tag{89}$$

cf. (80). This number equals either N given by (80) or $N+1$, because a sonic wave radiated by the shock front that reaches the piston is not necessarily able to catch up the shock front after its reflection. The dimensionless frequencies of these modes are

$$z_{2n-1} = \cosh\left(s_0 - (2n-1)q_s\right), \quad n = 1, 2, \ldots, N', \tag{90}$$

cf. (79). For the isolated shock case, only the $n = 1$ mode can be excited at the $x = 0$ surface because there is no reflection of sound from this surface back to the shock.

The asymptotic expression for the velocity perturbation is

$$\widetilde{v}_{xi}(t) \cong v_{xi}^{\infty} + \sum_{n=1}^{N'} v_{i,2n-1} \cos\left(\frac{z_{2n-1}}{z_0} \frac{k_x D t}{\sqrt{1-M_2^2}} \right), \tag{91}$$

where v_{xi}^{∞} is given by (88) and the oscillation amplitudes are

$$v_{i,1} = \frac{a_{20}\sqrt{z_1^2 - 1}}{z_1\left(z_0\sqrt{z_0^2 - 1} - a_{10}z_0^2 + a_{11}\right)};$$

$$v_{i,2n-1} = \frac{2(-1)^{n-1}a_{20}\sqrt{z_{2n-1}^2 - 1}}{z_{2n-1}\left(z_0\sqrt{z_0^2 - 1} - a_{10}z_0^2 + a_{11}\right)} \prod_{m=1}^{n-1} \frac{z_{2m}\sqrt{z_{2m}^2 - 1} + a_{10}z_{2m}^2 - a_{11}}{z_{2m}\sqrt{z_{2m}^2 - 1} - a_{10}z_{2m}^2 + a_{11}}, \qquad (92)$$

$2 \le n \le N'$.

For the isolated shock case, N' in (91) is replaced by the smaller of N' and 1. We see that the ripples at the free surface grow because of the RM-type instability developing on that surface. Superimposed on this linear growth are the oscillations induced by the waves radiated by the shock surface, which is forced to beat with a rhythm imposed by the longitudinal density modulation ahead of it. Similar arguments would apply to the case of a rigid boundary at $x = 0$. The difference is that for a rigid piston it is the sonic pressure and tangential velocity perturbations at $x = 0$ which would show the oscillations with the normalized frequency z_1. In the limit $k_x / k_y \to \infty$, $z_0 \to \infty$, $z_{2n-1}/z_0 \to [(1 - M_2)/(1 + M_2)]^{n-1/2}$, and the sum over *n* in (91) is reduced to the solution (37) and (38).

Figure 9 is plotted for an isolated shock wave interacting with a "quilt" pre-shock density modulation, Fig. 1(b). In the long-wavelength case, when (26) is satisfied, the periodic shock oscillations do not generate running waves that can reach the $x = 0$ surface. Therefore the longitudinal velocity perturbation amplitude at $x = 0$ approaches the constant asymptotic value given by Eq. (88), similarly to all other examples of the RM-type instability.[1, 16] It is illustrated by Fig. 9(a) plotted for $k_x / k_y = 1/5$, $g = 5/3$, $M_1 = 10$; the *x*-velocity perturbation amplitude V_p is normalized with respect to $e_k D$. The constant asymptotic value of V_p means that the initially planar contact interface

formed by the fluid particles initially located at $x = 0$ becomes rippled, with the ripple amplitude growing linearly with time, which is typical for the RM-type instabilities.[1] Figure 9(b) demonstrates a similar calculation for a short-wavelength "quilt," $k_x / k_y = 1$. In this case, the oscillating shock front radiates sonic waves that reach the $x = 0$ surface. As a result, its velocity V_p oscillates around the constant average value given by the same Eq. (88), rapidly approaching the asymptotic harmonic oscillation predicted by Eq. (91). In this case, too, the ripple amplitudes of the contact interface grow linearly with time, on the average, with a non-decaying oscillation superimposed upon the linear growth. This growth, however, is not easy to detect in either case, even in a simulation, unless it is done with a Lagrangian code that tracks individual fluid particles. Indeed, the unperturbed density is equal on both sides of the rippled interface, and therefore its growth is not captured by any diagnostic that tracks lateral mass redistribution, whether it is numerical or experimental, like face-on radiography.

2. Lateral mass redistribution

The lateral mass redistribution is a very important manifestation of all the interfacial instabilities, including RT, classical RM, ablative RM and other RM-type instabilities, which allows us to directly observe their development in laser targets with the aid of face-on x-ray radiography, as in Refs. 26-28. Our next example of the RM-type growth that involves the lateral mass redistribution refers to the "stripes" case of pre-shock density modulation, Fig. 1(a), with the free surface (constant pressure) boundary condition at the piston. The free surface is initially planar. However, the ripples rapidly develop at the surface because the shock wave driven by a constant pressure propagates faster into the lighter fluid, and the piston follows it. Then these ripples continue their

linear growth, similarly to all the RM-type situations.[1] Figure 10(a) shows the time history of the normalized ripple amplitude, kdx_p and of its velocity normalized as in Fig. 9, $V_p = d\left(kdx_p\right)/d\left(kDt\right)$. We see a good example of a RM-type behavior – linear asymptotic growth, constant velocity given by (88). Just as above, the growth is in the negative direction because the piston lags behind where the density is higher, $dr_k > 0$, see Fig. 2.

For our piston problem, the areal mass modulation amplitude dm can be expressed as

$$dm(t) = \frac{r_2 l}{2p}\left[-kdx_p + \frac{R-1}{R}kdx_s + k\int_0^{x_s}\left(\frac{dr(x,t)}{r_2} - \frac{\langle dr_1(t)\rangle}{r_1}\right)dx\right], \tag{93}$$

where the time-averaged value of the pre-shock density modulation at the shock front is defined as

$$\langle dr_1(t)\rangle = \frac{1}{t}\int_0^t dr_1(x = Dt')dt'; \tag{94}$$

e. g., for the "stripes" case $\langle dr_1\rangle / r_1 = e_k = const$, whereas for the "quilt" case (20) $\langle dr_1\rangle / r_1 = e_k \sin\left(k_x Dt\right)/\left(k_x Dt\right)$, cf. Refs. 1, 27, 28. The three contributions to dm in the square brackets come from the ripples at the piston surface and the shock front and from the density modulation left between the shock and the piston, respectively. The expression (93) accounts only for the time-dependent areal mass modulation resulting from the lateral mass redistribution, it does not include the constant initial mass modulation amplitude, which for the "stripes" case of Fig. 1(a) equals $dr_k L$, where L is the target thickness. According to (93), the negative growth of dx_p shown in Fig. 9(a)

adds a positive contribution to dm, as it should be – the bubble deepens where the density was initially low, thereby increasing the initial density contrast. In all situations of RM and RM-type growth, this contribution to dm from the unstable surface/interface rapidly becomes dominant, cf. Figures 1 of Refs. 27 and 28. Figure 10(b), however, shows that this is not the case here: at late time, we see a constant, finite difference between $(d/dt)dm$ (dm is normalized with respect to $r_2 l/2p$, kDt is the normalized time) and the constant asymptotic contribution from the RM-type unstable piston surface, $-V_p$. This difference cannot come from the shock front contribution, because the shock front displacement amplitude oscillates around a constant asymptotic value, as shown in Fig. 3, hence its time derivative is zero on the average. Therefore it is due to a lateral mass redistribution in the volume of the shocked target. Since the difference is negative, the perturbed lateral flow moves the mass from where the density was initially higher to where it was initially lower.

To elucidate the cause of this redistribution, consider the rigid piston boundary condition that eliminates any contribution of the perturbed surface to the areal mass modulation amplitude dm. Figure 11(a) shows the time history of dm for this case. The longer the shock wave propagates through the "stripes" density perturbation field, the more the initial amplitude $dr_k L$ is reduced by the post-shock flow. Figure 11(b) displays the profiles of relative density perturbation amplitude, $\tilde{r} = dr/r_2$, normalized with respect to e_k, at five instants of time. On the average, $\tilde{r}$ remains below unity (its pre-shock value shown by the horizontal dotted line), so the corresponding contribution to the right-hand side of (93) is negative. One can say that a shock wave helps the shocked fluid to reach greater uniformity by reducing the pre-shock density contrast in it; the shock

brings more pressure where the density is higher, and these areas expand. Note, however, that in the immediate vicinity of the shock front $\tilde{r}$ exceeds unity, and the direction of the lateral mass flow is different there. Indeed, the shock front is convex where the density is initially lower and concave where it is initially higher. It implies that the mass near the shock front flows laterally to where the density was initially higher, thereby adding a positive contribution to dm. The flow in the opposite direction dominates in the vicinity of the piston, and on balance the contribution reducing the post-shock density non-uniformity prevails.

What if the shock wave is driven by a laser, with an ablation front serving as a piston? In the case of a uniform target with front surface ripples, its instant shock loading produces the so-called ablative RM instability:[29] Instead of a linear growth similar to that illustrated by Fig. 10(a), both the ablation front displacement and areal mass modulation amplitudes exhibits slowly decaying oscillations. Such oscillations of dm have recently been observed experimentally.[26,27,30] Linear RM-type perturbation growth at the ablation front is suppressed by the "rocket effect"[19] that is incorporated in the boundary conditions (13), (14) – for details, see Refs. 1, 27, 29. For our case of the pre-shock "stripes" density perturbation, Fig. 1(a), the time histories of the normalized displacement amplitude of the ablation front, kdx_a, and of the areal mass modulation amplitude, dm, are shown in Fig.12 plotted for the parameters of the ablation front $r_D = 0.0625$, $M_a = 0.05$, which roughly correspond to a planar solid DT target with $l = 24$ μm ripples on its front surface irradiated with a 0.35 μm laser radiation at 3×10^{13} W/cm^2, see Ref. 31.

We see in Fig. 12(a) that the slowly decaying oscillations of the ablation front occur around a nonzero average. This happens because at early time the ablation front,

following the shock front, makes a dent in the target where its density was initially lower. Later, the dent remains, since the plasma in its vicinity stays non-uniform. The contribution of the rippled ablation front to the mass modulation amplitude dm does not decay, nor is dominant, as in the case of a rippled uniform target.[1, 26, 27, 29] Rather, Fig. 12(b) demonstrates that the mass flow in the volume reducing the density contrast, dominates here, similarly to the case of a rigid piston, cf. Fig. 11(a).

3. Pre-shock density modulation localized near the shocked surface

One of the issues that could be addressed studying shock propagation in a fluid with weakly modulated density refers to numerical simulations of the RM-type unstable flows. In laser fusion studies, one often has to model a very small roughness of the irradiated surface. It is not easy to resolve very small-amplitude ripples on a numerical grid. A typical remedy for it is to consider a planar surface and introduce a density perturbation in the volume. For example, a sine-wave ripple of amplitude dx_0 and lateral wavenumber k on the front surface of the target whose density is r_1 can be approximated by a density profile at $x \geq 0$:

$$\frac{r(x,y)}{r_1} = 1 + dx_0 f(x)\cos(ky), \tag{95}$$

where $f(x)$ is a dimensional function ($[f]$=cm^{-1}) localized near the surface, which satisfies the normalization condition

$$\int_0^\infty f(x)dx = 1. \tag{96}$$

This condition ensures that the initial areal mass modulation amplitude in this flat target with inner density modulation equals $r_1 dx_0$, the same as in a uniform target of density r_1 with a single-mode surface ripple whose amplitude is dx_0.

For example, we can consider profiles peaked at the surface ($n = 0$) or near it ($n > 0$) and exponentially decaying far from it

$$f(x) = \frac{q}{n!}(qx)^n \exp(-qx), \quad n \geq 0, \tag{97}$$

or Bessel-function profiles, exhibiting a slow oscillatory decay with increased x:

$$f(x) = qJ_0(qx). \tag{98}$$

All the profiles (97) and (98) satisfy the normalization condition (96). Increasing the parameter q, one can make these perturbations more and more localized near the front surface, which is compatible with relative smallness of density perturbation provided that the equivalent ripple amplitude dx_0 is sufficiently low. Of course, the problem is determined by the dimensionless ratio q/k. Apparently, in the limit $q/k \to \infty$, the density perturbation becomes localized near the surface on the length scale much less than $l = 2p/k$, the wavelength of the transverse ripple. The questions are whether in this limit the internal density modulation is equivalent to the surface ripple as far as the later-time perturbation dynamics is concerned, and if it is then how large should the ratio q/k be so that we can make use of this equivalence in the simulations.

Instantly loading a free rippled surface with a constant pressure, we generate a RM-type instability at this surface. A similar effect arises from loading a planar surface with a single-mode density perturbation near the loaded surface. Let us compare the results. Figure 13 shows the normalized growth rate of the areal mass variation amplitude

(in units of $r_1 dx_0$) and its time derivative vs. normalized time, kDt, for the $n = 0$, purely exponential (a), and Bessel-function (b) profiles of the areal density perturbation near the surface. For both cases, the ratio q/k varies in the range from 1 to 4, $g = 5/3$, $M_1 = 10$.

We see that the convergence to the surface ripple case with increasing q/k is faster for the Bessel-function profile compared to the exponential. This is because the former concentrates a larger part of the (positive) density perturbation in the vicinity of the surface compared to the latter. At larger distance the density perturbation becomes negative, but it turns out to have less effect on the surface RM-type growth.

IV. NUMERICAL SIMULATIONS

The theoretical results presented above are exact and therefore do not require numerical verification. Rather, as in our earlier work,[4, 31, 32] they can be helpful in testing the accuracy of the codes.

Our simulations were performed in two dimensions using the Eulerian FAST2D hydrocode developed at the Naval Research Laboratory[33] (more details and further references are given in Ref. 31). Two profiles of laterally periodic pre-shock density modulation were simulated: the "stripes" case of Fig. 1(a), and the density modulation (97) localized near the target surface. All our simulations were done for a strong shock wave $M_1 = 10$, driven into an ideal gas $g = 5/3$ by a rigid piston, whose velocity was $V_p = 4 \times 10^6$ cm/s. The lateral perturbation wavelength in all cases was taken $l = 30$ μm. Dimensions of the simulation box were one full wavelength $l = 30$ μm in the lateral (y) direction and 200 μm in the longitudinal (x) direction. The rectangular grid was fixed in space and time; its cell size was 0.5 μm in the longitudinal direction and 0.9375

μm in the lateral direction, which corresponds to 32 zones per wavelength (about as much or more than one can afford in multi-mode inertial confinement fusion (ICF) relevant simulations[34]).

Figure 14 compares numerical simulation results and the theory for the "stripes" case. The relative density modulation amplitude $e = dr / r_1$ is varied between 5×10^{-4} and 5×10^{-2}. The areal mass modulation amplitude is normalized with respect to its initial value, $dm_0 = Ldr$, where $L = 200$ μm. The theoretical line in Fig. 14 is basically the same as in Fig. 11(a), differing only in normalization of *dm* (vertical axis) and in time units (horizontal axis). Figure 14(a) presents the results obtained with a time step initially chosen $\Delta t_0 = 0.1$ ps. This appears to be a reasonable choice, given that $V_p \Delta t_0 / l = 1.3\times10^{-4}$. In the simulations of similar problems done for the ICF-relevant conditions,[2, 3, 5] where the laser intensity increases gradually, the code automatically adjusts its time step to fit the problem. In our present problem, the shock wave of full strength is generated instantly. The code was not originally written for introducing instant shocks, so that the initial step needs to be prescribed. We see, however, that our simulation results deviate from the exact theoretical results from the very beginning. The deviation is not healed with the passage of time, as the shock wave propagates in the longitudinal direction for up to 7 lateral wavelengths. Moreover, the deviation between the exact solution and the numerical results grows linearly with time. Figure 14(a) illustrates that this deviation cannot be attributed to nonlinear effects due to finite amplitude of the pre-shock density modulation: reduction of the parameter *e* by two orders of magnitude does not bring the numerical result closer to the theory.

What matters here is a proper choice of the initial time step. Taking the initial time step $\Delta t_0 = 1$ fs and allowing it to increase no more than by 5% per time step, we obtain the results shown in Fig. 14(b). This choice is seen to make the agreement with the theory much better; in particular, the average growth rate of dm is modeled very accurately for both values of the initial density modulation amplitude, 2.5×10^{-3} and 10^{-2}, even though the time step after the first 1 ns becomes the same as in the simulations illustrated by Fig. 14(a).

Figure 15 shows a similar comparison for the localized density modulation (95) and (97). Here, we have chosen $q = k = 2p$ /(30 μm) and did the simulations for the parameter n in (97) varied from 0 to 4. For all the profiles, the same value of $dx_0 = 0.1$ μm in (95) was chosen, corresponding to the initial value of mass modulation amplitude $dm_0 = r_1 dx_0$; areal mass modulation amplitudes are shown normalized with respect to this value. The maximum value of the relative density modulation amplitude in the profile (97) equals $(2pdx_0 / l)\times n^n e^{-n} / n!$, and for n increased from 0 to 4 it decreases from 2×10^{-2} to 4×10^{-3}, which, as confirmed by Fig. 14(b), is sufficiently small for the linear theory to be applicable. Our theory, as demonstrated by Fig. 15(a), predicts for all cases oscillations around an average value, which is less than unity. This is consistent with our previous results (Fig. 11): the shock passage decreases the average lateral non-uniformity of the density distribution.

Here again, Fig. 15(b) shows that the simulation started with a too large time step $\Delta t_0 = 0.1$ ps yields a result, which is qualitatively incorrect, and its deviation from the exact solution grows linearly with time. The choice of a very small initial time step

$\Delta t_0 = 1$ fs, helped to improve the agreement, see Fig. 15(c). However, even in the latter case our numerical modeling displays a slow negative linear growth of *dm*, which should not be there: it is a numerical artifact.

V. CONCLUSIONS

We have developed a small-amplitude theory describing the interaction of planar, constant-strength shock waves with pre-shock non-uniformities distributed in the volume of a shocked fluid. This theory describes the distortion of the shock front and the post-shock flow, including the lateral mass redistribution. Predictions of our theory are in good qualitative agreement with the known results of numerical simulations. For example, a shock wave was shown to "mix" low- and high-density mass, thus reducing the average density non-uniformity in a shocked volume, in an agreement with the simulations of Ref. 7, where a foam-like medium was modeled. For a "joint" pre-shock density perturbation, localized in one transverse direction, the leading edge of the distorted shock wave was found to remain localized near the "joint" and maintain a constant curvature/length scale determined by the joint width, whereas the shock front as a whole approaches a self-similar shape, in agreement with the numerical results of Ref. 8, where a laser target containing an actual joint was modeled. A slightly simpler behavior was found for a "tube" pre-shock density perturbation, localized in both transverse directions: the shock front distortion is finite and contained in the vicinity of the "tube," whereas the RM-type growth of the areal mass modulation, not being limited, remains localized, in agreement with the numerical results obtained in Ref. 9 for laser targets with feeding tubes.

The importance of our results stems from the fact that these details of shock distorting and post-shock behavior have been quantified and described by exact analytical solutions. Such solutions are very helpful for testing the accuracy of the hydrodynamic simulation codes, particularly when such codes must be used to model the growth of perturbations starting from their very small initial amplitudes. Small-amplitude perturbations are notoriously hard to resolve, and there is always a risk either to contaminate the simulation results with a numerical noise or to damp them heavily with a numerical dissipation.[31] Our numerical examples with small pre-shock density perturbations demonstrate that it does not take much for the numerical solution to deviate from the exact analytical solution, and that in the absence of acceleration this numerical error tends to grow linearly with time, in a RM-type fashion. Unless the code has been thoroughly tested in this regime, such deviations are likely to remain undetected in realistic multi-mode simulations, where the exact solution is unknown.

For the constant-strength shocks propagating into a uniform (on the average) density target, the theory is essentially complete. It is very important to generalize it for shock waves whose strength decreases with time, including those propagating up the density gradients in the laser targets. This advancement is needed make the theory directly applicable to the situations relevant for laser imprint suppression and adiabat shaping with the aid of a spike pre-pulse producing a shock-rarefaction flow.[2, 3, 5] Exact and approximate analytical results of the linear stability analysis obtained for the related cases of impulsive loading[4] and Vishniac instability of a blast wave,[35] respectively, indicate feasibility of this development.

ACKNOWLEDGMENTS

A. L. V., N. M., S. T. Z. and A. J. S. are supported by the U. S. Department of Energy, Defense Programs, J. W. G. by the Ministry of Educacion y Ciencia (FIS 2006-05389) and Consejo de Comunidades de Castilla-La Mancha of Spain (PAI-05-045), and C. H. R. de L. by Ministry of Educación y Ciencia (Beca-Colaboración 2006/07).

APPENDIX: DERIVATION OF THE LAPLACE-TRANSORMED SOLUTIONS

When the shock wave is driven by a piston starting from $t = 0$, we impose the boundary condition (11) or (12) at $x = 0$ for all time. This boundary condition requires the existence of reflected pressure waves in the positive *x*-direction, following the shock front. As a consequence, the Laplace transform for the shock pressure perturbations has to be obtained from an inhomogeneous functional equation.[16, 22, 24] Due to this, the mathematical structure of the solution in a general case cannot be presented by a simple closed expression like that of Eqs. (43) and (68). The actual formula for $\widetilde{P}_s$ consists of an infinite sum of more or less complicated functions. Each term in the sum appears as a consequence of the multiple reverberations of sonic waves that take place between the shock surface and the piston. For such boundary condition, we consider the full problem of the "quilt" pre-shock density modulation. After some algebra, using the method described in Ref.16, it can be shown that the pressure function $\widetilde{P}_s$ is the solution of a functional equation:[16]

$$\widetilde{P}_s(q) = l_1(q) + l_2(q)\widetilde{P}_s(q + 2q_s), \tag{A1}$$

where the Laplace-transform variable *s* is related to q by $s = \sinh q$. The characteristic that makes the above equation more difficult to solve is the fact that the argument of the

pressure is "shifted" by the amount $2q_s$ in the right-hand-side of Eq. (A1). This shift in the equation is necessary to take into account the multiple reverberations between the shock and the piston, and the Doppler shift that occurs after each reflection at the shock surface.[24] The functions $l_1(q)$ and $l_2(q)$ for the double-periodic "quilt" pre-shock density modulation, with rigid piston, free surface or isolated shock boundary conditions, are:

$$l_1(q) = \frac{a_2(q) + R_p a_2(q + 2q_s)}{\cosh q - a_1(q)}, \quad l_2(q) = R_p \frac{a_1(q + 2q_s) + \cosh(q + 2q_s)}{\cosh q - a_1(q)}, \tag{A2}$$

where

$$a_1(q) = a_{10} \sinh q + \frac{a_{11}}{\sinh q}, \quad a_2(q) = -a_{10} \tilde{p}_{s0} + \frac{a_{20}}{\sinh^2 q + z_0^2}. \tag{A3}$$

Here R_p is the reflection coefficient for sonic waves incident upon the piston ($R_p = 1$, -1, and 0 for the rigid piston, free surface and isolated shock boundary conditions, respectively), and $\tilde{p}_{s0}$ is the initial pressure perturbation amplitude at the piston surface. Its value for the rigid piston boundary condition is obtained from the perturbed Rankine-Hugoniot equations evaluated at $t = 0^+$:

$$\tilde{p}_{s0} = \epsilon_k \frac{M_1^2 M_2^2}{M_1^2 + 1}(R - 1); \tag{A4}$$

for the free surface boundary condition, $\tilde{p}_{s0} = 0$, as follows from (12), and for the isolated shock boundary condition it is given by (48).

The solution to Eq. (A1) is the sum of a solution of the homogeneous equation plus a particular solution. As our gas has an ideal EOS, it is not difficult to see that the

only acceptable solution to the homogeneous equation is the trivial zero function.[24] An exact particular solution of (A1) is easily obtained by iterations:[16]

$$\widetilde{P}_s(q) = l_1(q) + \sum_{n=1}^{\infty} l_1(q + 2nq_s) \prod_{m=0}^{n-1} l_2(q + 2mq_s) . \qquad \text{(A5)}$$

With another EOS, different from an ideal gas, the homogeneous equation could contribute with a non-zero solution and therefore, another modes could be excited at the shock surface.[24] For the case of isolated shock boundary condition, $R_p = 0$, and therefore all the terms with shifted arguments $q + 2q_s$ describing reverberations in (A2), (A3) vanish, so that $l_2(q) \equiv 0$. Hence in the right-hand side of (A5) only the first term remains, and this solution is reduced to (68), or, in a particular case of the "stripes" pre-shock density modulation, to (43). For other boundary conditions, the inversion of (A5) needed to get the complete temporal evolution requires the evaluation of a sufficiently large number of terms, similarly to the case of the classical RM instability studied in Ref. 16, hence the temporal solution could be rather complicated. Usually, few terms are sufficient. We can calculate the complete temporal evolution starting from $t = 0^+$ by two different procedures: using the original functional equation (A1) or its exact solution provided by Eq. (A5). If we expand $\widetilde{P}_s(q)$ into a power series in $\exp(-q)$ and substitute it into Eq. (A1), as suggested for the first time by Zaidel,[22] we could equate powers of $\exp(-q)$ and get the complete temporal solution in the whole fluid as a series of Bessel functions of integer order, because the inverse Laplace transform of the n^{th} integer power of $\exp(-q)$ is $nJ_n(r_s)/r_s$, where r_s is given by (50). An alternative way consists of truncating Eq. (A5) at some order and constructing an integral representation of the pressure perturbations at the shock front, as was done for the isolated shock boundary

condition, see Eqs. (49), (55) and (58). It must be taken into account that the order of truncation will depend on the value of q_s, which is a monotonically decreasing function of M_1. As the shock strength increases, more terms should be retained, at least to accurately describe the sonic reverberations and the vorticity/entropy generation behind the shock front, when the shock is not very far from the surface $x = 0$. To do this, we must construct an auxiliary function $f_p(z)$ [as in Eqs. (49), (55) and (58)], that would be essentially the imaginary part of $\widetilde{P}_s(iz)$ evaluated at both sides of the imaginary axis along the segment $[-i, i]$, with the multi-valued character of expressions like $\sqrt{s^2+1}$ properly taken into account. It is quite clear that more complicated boundary conditions result in more complicated mathematical structure of the function $f_p(z)$. In the case of an isolated shock, we have obtained a very simple closed form expression for this auxiliary kernel. This may not be so for the rigid piston boundary, as the algebraic complexity of $f_p(z)$ will depend on the level of truncation of the infinite series given by Eq. (A5). Nevertheless, despite of these algebraic complications, the exact solution given by Eq. (A5) shows its power and beauty in providing us with important information on the behavior at large times.

For the long-wavelength regime, $z_0 < 1$, it is easy to see that we obtain the same final asymptotic behavior as in the isolated shock case, given already in Eqs. (32) and (61). The only substantial difference between the isolated shock and the rigid piston case lies in the amplitudes of the temporal decaying terms. But once this transient behavior becomes negligible, the final oscillatory response is the same for both cases, independently of the boundary conditions far downstream of the shock surface. In this

regime, the only term that contributes with an oscillatory asymptotic is the first term that appears in $l_1(q)$:

$$\frac{a_{20}}{\sinh^2 q + z_0^2} \frac{1}{\cosh q - a_1(q)}, \tag{A6}$$

with two poles at $s = \pm i z_0$. This expression reproduces the exact solution to the isolated shock problem, Eq. (68), which explains why the asymptotic expressions coincide in the long-wavelength regime. The other terms that appear in Eq. (A5) are due to the multiple reverberations that occur between the rigid wall and the shock surface and their contribution for large times is an oscillation with an amplitude that decays as $t^{-3/2}$. These additional terms are actually negligible for very weak shocks because $q_s \cong -(1/2)\ln(M_1 - 1) \to \infty$ as M_1 approaches unity, making those terms less important than the one shown in Eq. (A6).

However, within the remaining terms that represent the multiple reverberations of the sonic waves in Eq. (69), we recognize contributions of the form:

$$\frac{a_{20}}{\sinh^2(q + 2q_s) + z_0^2} \frac{1}{\cosh(q + 2q_s) - a_1(q + 2q_s)}. \tag{A7}$$

Higher-order terms like one shown in Eq. (A7) (involving functions with arguments of the shifted form $q + 4q_s$, $q + 6q_s$, etc.) might contribute pure imaginary poles. These poles are imaginary roots of the equation $\sinh^2(q + 2nq_s) + z_0^2 = 0$, with $n \geq 1$ any positive integer; they add "extra" non-decaying oscillations at normalized frequencies lower than z_0. Indeed, we find two such terms, with a shift equal to $2q_s$ for $n = 1$. Those terms contribute pure imaginary poles in the short-wavelength regime, when not only $z_0 > 1$, but also a stricter condition (77) is satisfied. The number *N* of these poles is given

by Eq. (80). Non-decaying oscillations corresponding to the shock front perturbation amplitudes from the poles are given by the $n = 1, 2, \ldots, N$ terms of the sums (81), (82). The value of n for each of these terms corresponds to the number of reflections from the piston.

For the free surface boundary condition, the piston surface $x = 0$ after $t = 0^+$ becomes a vortex sheet, which exhibits a RM-type instability.[1] It is not difficult to arrive to a formula for the asymptotic growth rate at the rippled surface/interface, which is valid both for the isolated shock case and for the free surface case in the long-wavelength regime. The calculations are similar to those outlined in detail in Ref. 16. We obtain the following expression for the Laplace transform of the ripple x-velocity at $x = 0$:

$$\widetilde{V}_{xi}(q) = \frac{1}{\sinh q}\left\{\widetilde{v}_{xi}^{0+} - [\cosh(q+q_s) + a_1(q+q_s)]\widetilde{P}_s(q+q_s) - \frac{a_{20}}{\sinh^2(q+q_s) + z_0^{\,2}}\right\}, \quad \text{(A8)}$$

where the velocity perturbation at $t = 0^+$ is defined below Eq. (88) . The Laplace transform (A8) shows a pole at $s = 0$, giving rise to a constant asymptotic rate of linear growth.[16] It also can have imaginary poles at z_1, z_3 …, describing sonic oscillations, when the conditions for those oscillations to exist are satisfied: $s_0 > (2n-1)q_s$, $n = 1, 2, \ldots$, cf. (78). Their number is given by (89), and their normalized frequencies - by (90). The asymptotic time dependence corresponding to (A8) is given by (91).

References

[1] A. L. Velikovich, J. P. Dahlburg, A. J. Schmitt *et al*., Phys. Plasmas **7**, 1662 (2000).

[2] N. Metzler, A. L. Velikovich, A. J. Schmitt and J. H. Gardner, Phys. Plasmas **9**, 5050 (2002).

[3] V. N. Goncharov, J. P. Knauer, P. W. McKenty *et al*., Phys. Plasmas **10**, 1906 (2003); K. Anderson and R. Betti, Phys. Plasmas **10**, 4448 (2003); R. Betti, K. Anderson, J. Knauer *et al*., Phys. Plasmas **12**, 042703 (2005).

[4] A. L. Velikovich, A. J. Schmitt, N. Metzler, and J. H. Gardner, Phys. Plasmas **10**, 3270 (2003).

[5] N. Metzler, A. L. Velikovich, A. J. Schmitt *et al*., Phys. Plasmas **10**, 1897 (2003).

[6] S. E. Bodner, D. G. Colombant, J. H. Gardner *et al*., Phys. Plasmas **5**, 1901 (1998); S. E. Bodner, D. G. Colombant, A. J. Schmitt, and M. Klapisch, Phys. Plasmas **7**, 2298 (2000); S. E. Bodner, D. G. Colombant, A. J. Schmitt *et al*., Fusion Engineering and Design **60**, 93(2002).

[7] G. Hazak, A. L. Velikovich, J. H. Gardner, and J. P. Dahlburg, Phys. Plasmas **5**, 4357 (1998).

[8] S. R. Goldman, S. E. Caldwell, M. D. Wilke *et al*., Phys. Plasmas **6**, 3327 (1999).

[9] J. Edwards, M. Marinak, T. Dittrich *et al*., Phys. Plasmas **12**, 056318 (2005).

[10] *The Effects of Nuclear Weapons*, edited by S. Glasstone, U. S. Dept. of Defense and U. S. Department of Energy (U. S. Gov. Print Off., Washington, DC, 1964), Section 3.35; M. A. Sadovskii and V. V. Adushkin, Dokl. Akad. Nauk SSSR **300**, 79 (1988).

[11] V. I. Bergel'son, I. V. Nemchinov, T. I. Orlova, Sov. Phys. Dokl. **32**, 691 (1987); V. I. Artem'ev, V. I. Bergel'son, S. A. Medveduk *et al*., Fluid Dyn. **31**, no. 1, 121 (1996).

[12] R. G. Shreffler and R. H. Christian, J. Appl. Phys. **25**, 324 (1954); R. E. Duff and F. I. Peterson, *ibid*. **51**, 3957 (1980); M. A. Tsikulin, E. G. Popov, *Radiative Properties of Shock Waves in Gases* (in Russian) (Moscow, Nauka, 1977).

[13] J. Grun, R. Burris, G. Joyce *et al*., J. Appl. Phys. **83**, 2420 (1998).

[14] A. L. Velikovich and M. A. Liberman, JETP Lett. **27**, 420 (1978).

[15] R. D. Richtmyer, Commun. Pure Appl. Math. **13**, 297 (1960).

[16] J. G. Wouchuk, Phys. Rev. E **63**, 056303 (2001).

[17] J. G. Wouchuk, Phys. Plasmas **8**, 2890 (2001).

[18] L. D. Landau and E. M. Lifshitz, *Fluid Mechanics* (Pergamon, New York, 1987).

[19] J. Sanz, Phys. Rev. Lett. **73**, 2700 (1994); A. R. Piriz, J. Sanz, and F. L. Ibañez, Phys. Plasmas **4**, 1117 (1997).

[20] N. Metzler, A. L. Velikovich, and J. H. Gardner, Phys. Plasmas **6**, 3283 (1999).

[21] See National Technical Information Service Document PB2004-100597 [A. E. Roberts, Los Alamos Scientific Laboratory Report No. LA-299, 1945]. Copies may be ordered from the National Technical Information Service, Springfield, VA 22161.

[22] P. M. Zaidel, J. Appl. Math. Mech. **24**, 316 (1960); Iu. M. Nikolaev, ibid. **29**, 785 (1965); N. C. Freeman, Proc. Roy. Soc. A **228**, 341 (1955).

[23] M. G. Briscoe and A. A. Kovitz, J. Fluid Mech. **31**, 529 (1968); A. A. Kovitz and M. G. Briscoe, J. Acoust. Soc. of America **45**, 1157 (1969).

[24] J. G. Wouchuk and J. L. Cavada, Phys. Rev. E **70**, 046303 (2004).

[25] J. W. Bates, Phys. Rev. E **69**, 056313 (2004).

[26] Y. Aglitskiy, A. L. Velikovich, M. Karasik *et al*., Phys. Rev. Lett. **87**, 265001 (2001).

[27] Y. Aglitskiy, A. L. Velikovich, M. Karasik *et al*., Phys. Plasmas **9**, 2265 (2002).

[28] Y. Aglitskiy, N. Metzler, M. Karasik *et al*., Phys. Plasmas **13**, 080703 (2006).

[29] V. N. Goncharov, Phys. Rev. Lett. **82**, 2091 (1999).

[30] O. V. Gotchev, V. N. Goncharov, J. P. Knauer *et al*., Phys. Rev. Lett. **96,** 115005 (2006).

[31] S. T. Zalesak, A. J. Schmitt, J. H. Gardner, and A. L. Velikovich, Phys. Plasmas **12**, 056311 (2005).

[32] A. L. Velikovich, S. T. Zalesak, N. Metzler, and J. G. Wouchuk, Phys. Rev. E **72**, 046306 (2005).

[33] J. P. Boris and D. L. Book, J. Comput. Phys. **11**, 38 (1973); also see *Solution of the Continuity Equation by the Method of Flux-Corrected Transport, Methods in Computational Physic*s (Academic, New York, 1976), Vol. 16, pp. 85-129.

[34] A. J. Schmitt, A. L. Velikovich, J. H. Gardner *et al*., Phys. Plasmas **8**, 2287 (2001).

[35] D. Ryu and E. T. Vishniac, Astrophys. J. **313**, 820 (1987).

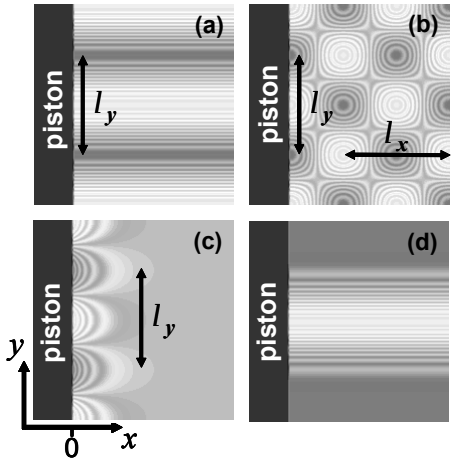

Figure 1. Density maps showing examples of the pre-shock density modulation: (a) periodic in the lateral direction ("stripes"); (b) periodic in both lateral and longitudinal directions ("quilt"); (c) periodic in the lateral direction and concentrated near the surface; (d) non-periodic, Gaussian density profile in the lateral direction.

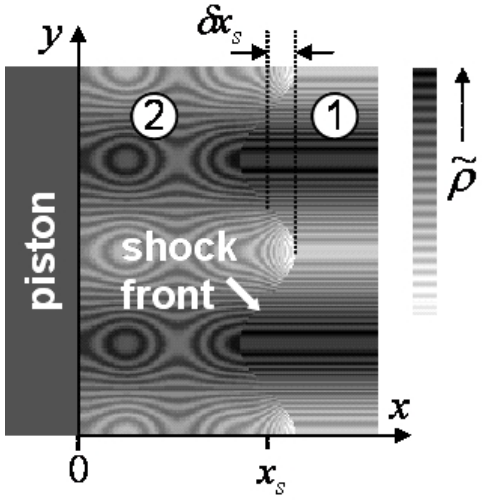

Figure 2. Density perturbation map illustrating formulation of the problem for the "stripes" case of Fig. 1(a). The shock wave is driven by a rigid piston in the positive x direction. Density modulation of the pre-shock fluid 1 is periodic in y, independent of time and the longitudinal coordinate x. The flow of the shocked fluid 2 is non-steady and x-dependent but maintains the original periodicity in the lateral direction y. The shape of the perturbed shock front is a single-mode sine wave whose amplitude is denoted by dx_s.

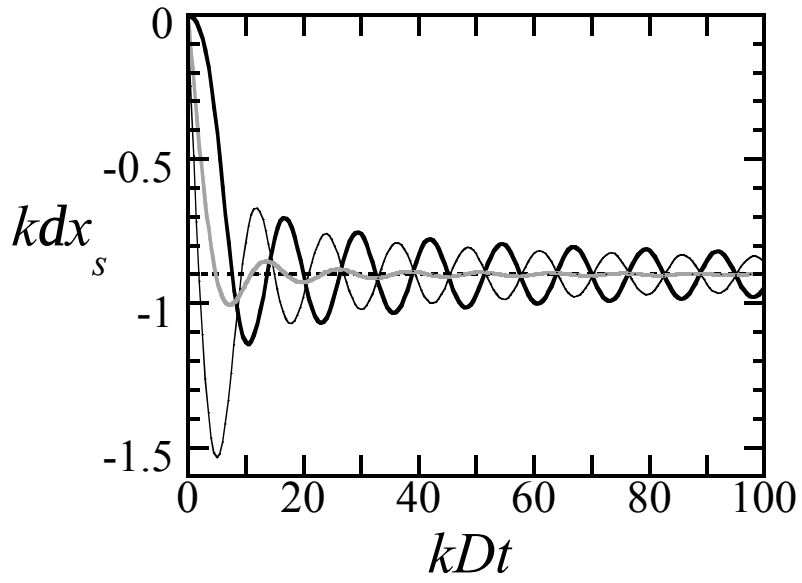

Figure 3. Normalized shock ripple amplitude kdx_s vs. normalized time kDt for the "stripes" case of the pre-shock density modulation, $g = 5/3$, $M_1 = 10$. Dotted line displays the asymptotic value (34), thick, thin and gray solid lines correspond to the rigid piston, free surface and isolated shock boundary conditions, respectively.

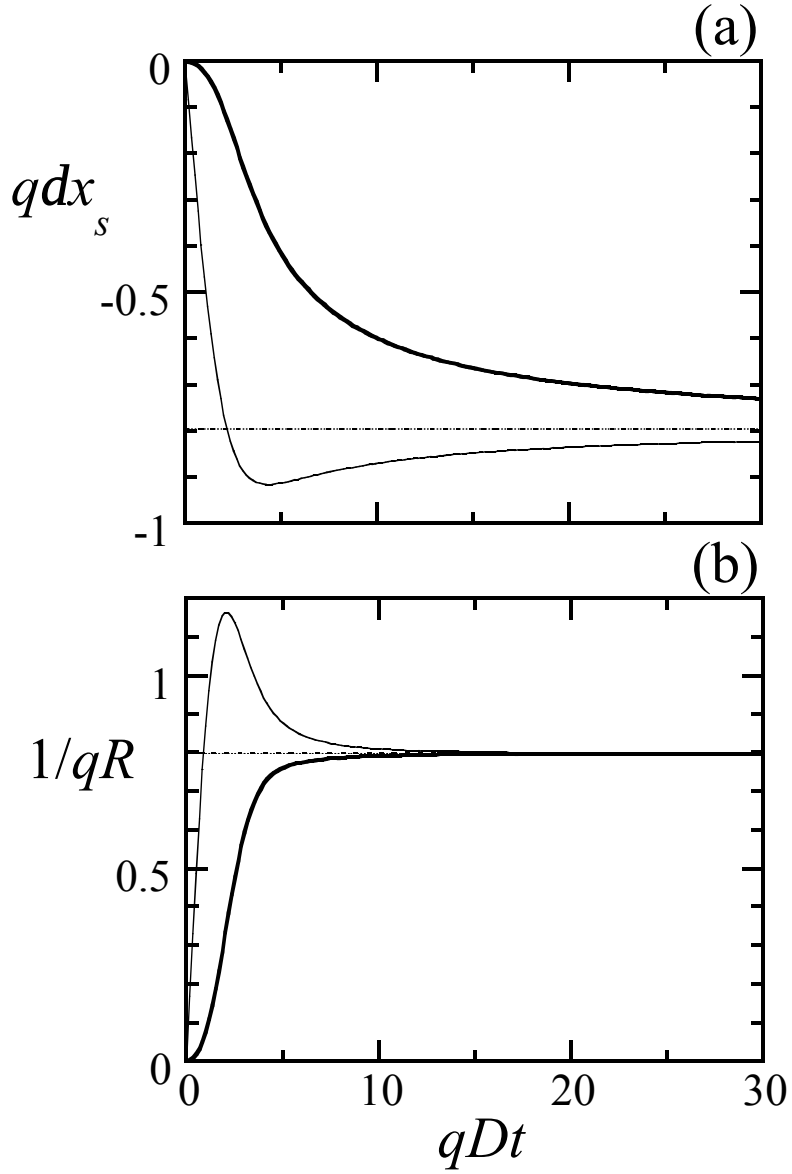

Figure 4. Normalized shock displacement amplitude qdx_s (a) and normalized curvature of the shock front $1/qR$ at $r = 0$ (b) vs. normalized time qDt for the cylindrical Gaussian "tube" localized pre-shock density perturbation, $g = 5/3$, $M_1 = 10$. Thick and thin solid lines correspond to the rigid piston and free surface boundary conditions at the piston surface, respectively. Horizontal dotted lines show the asymptotic values (60) and (61).

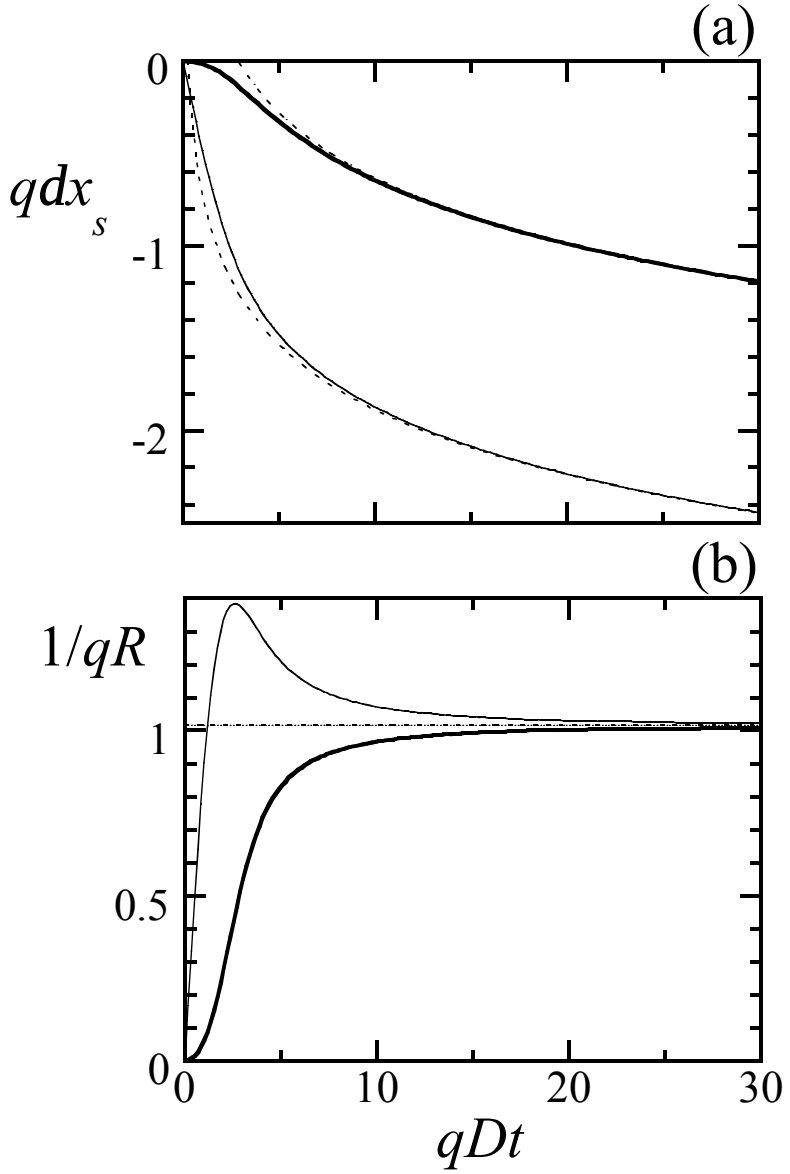

Figure 5. Normalized shock displacement amplitude qdx_s (a) and normalized curvature of the shock front $1/qR$ at $y = 0$ (b) vs. normalized time qDt for the planar Gaussian "joint" localized pre-shock density perturbation, $g = 5/3$, $M_1 = 10$. Thick and thin solid lines correspond to the rigid piston and free surface boundary conditions at the piston surface, respectively. Dotted lines in (a) show the asymptotic formulae (66) for each boundary condition; horizontal dotted line in (b) shows the asymptotic curvature (67).

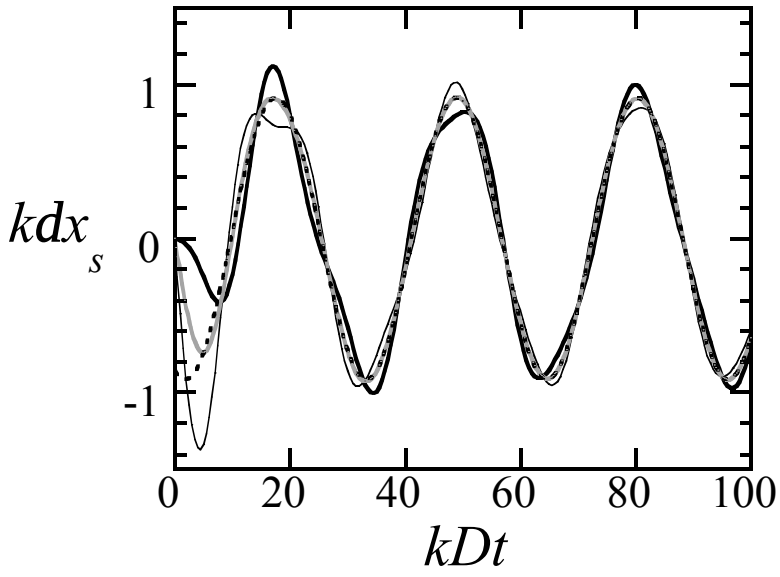

Figure 6. Normalized shock ripple amplitude kdx_s vs. normalized time kDt for the long-wavelength "quilt" case of the pre-shock density modulation, $g = 5/3$, $M_1 = 10$, $k_x / k_y = 1/5$. Dotted line displays the asymptotic formula (35), thick, thin and gray solid lines correspond to the rigid piston, free surface and isolated shock boundary conditions, respectively.

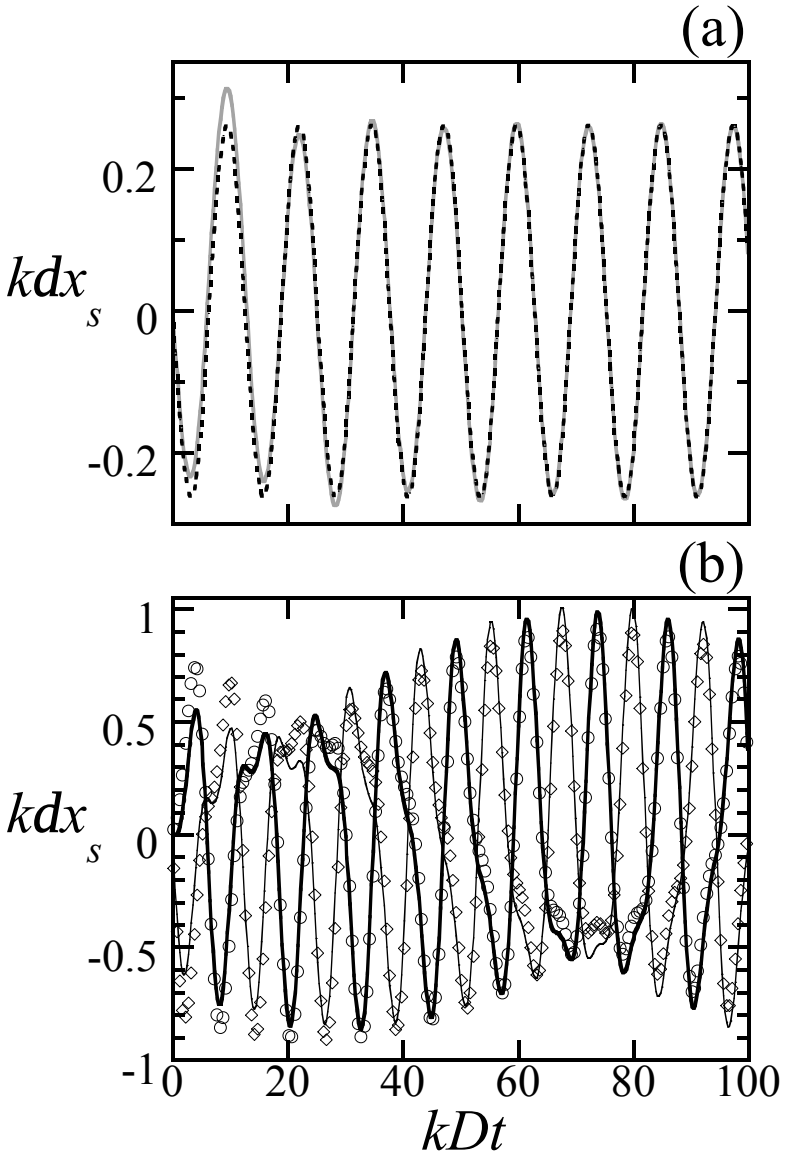

Figure 7. Normalized shock ripple amplitude kdx_s vs. normalized time kDt for the short-wavelength "quilt" case of the pre-shock density modulation: $g = 5/3$, $M_1 = 10$, $k_x / k_y = 1$: (a) Dotted line displays the asymptotic formula (35), gray line – the exact solution for isolated shock. (b) Thick and thin solid lines correspond to the exact solution for rigid piston and the free surface boundary conditions, respectively, circles and diamonds – to Eq. (82) with $R_p = 1$ and -1, respectively.

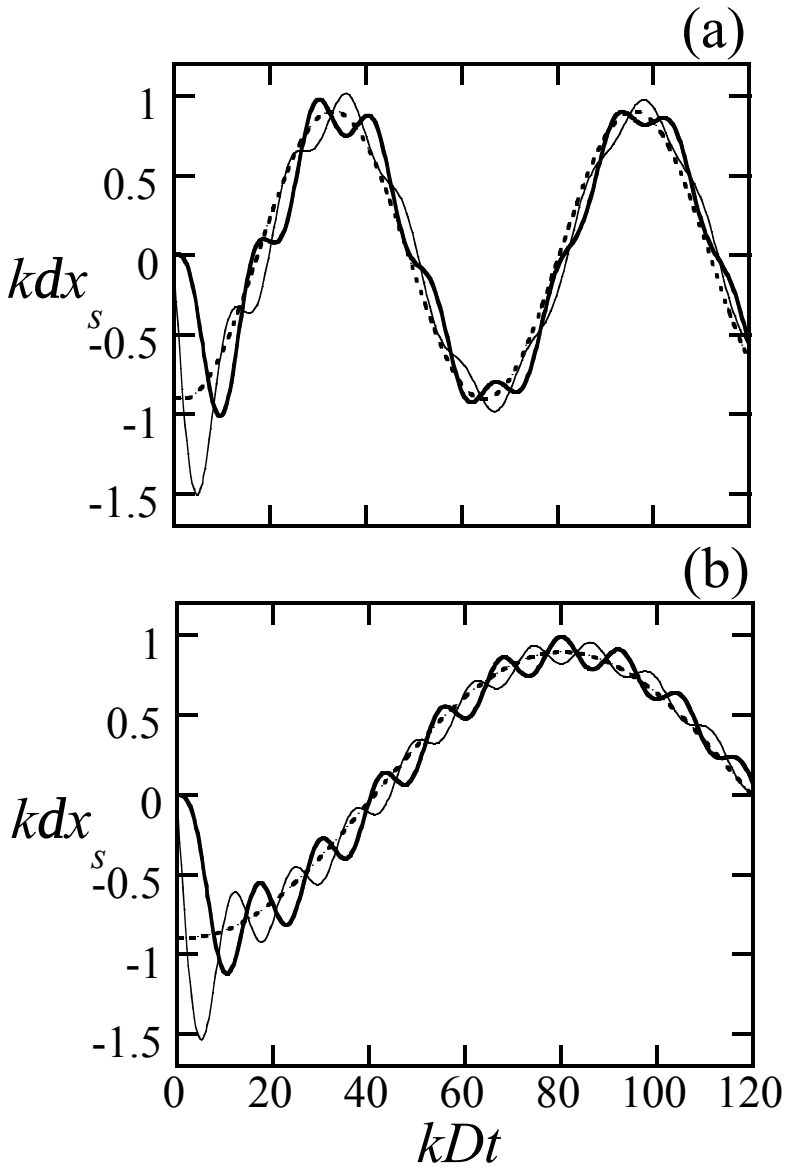

Figure 8. Normalized shock ripple amplitude kdx_s vs. normalized time kDt for the pre-shock standing sonic wave, $g = 5/3$, $M_1 = 10$ (a) and $M_1 = 25$ (b). Dotted line displays the asymptotic shape (32), thick and thin solid lines correspond to the rigid piston and free surface boundary conditions at the piston surface, respectively.

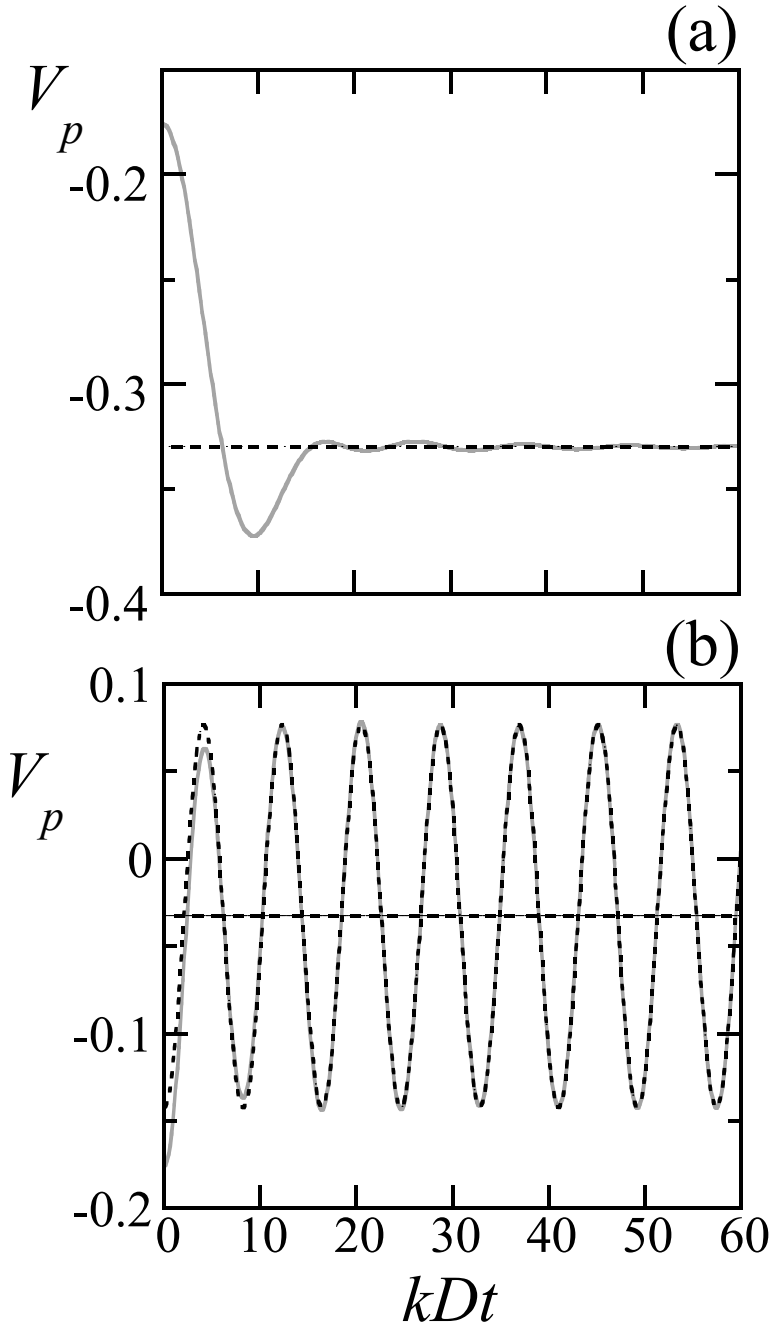

Figure 9. Longitudinal velocity perturbation amplitude at $x = 0$ vs. normalized time kDt for an isolated shock wave interacting with a "quilt" pre-shock density perturbation shown as gray line. (a) Long-wavelength regime, $k_x / k_y = 1/5$; horizontal dashed line – late-time asymptotic value given by (88). (b) Short-wavelength regime, $k_x / k_y = 1$; dotted line - late-time asymptotic oscillations given by (91), horizontal dashed line – average late-time value given by (88). For both cases, $g = 5/3$, $M_1 = 10$.

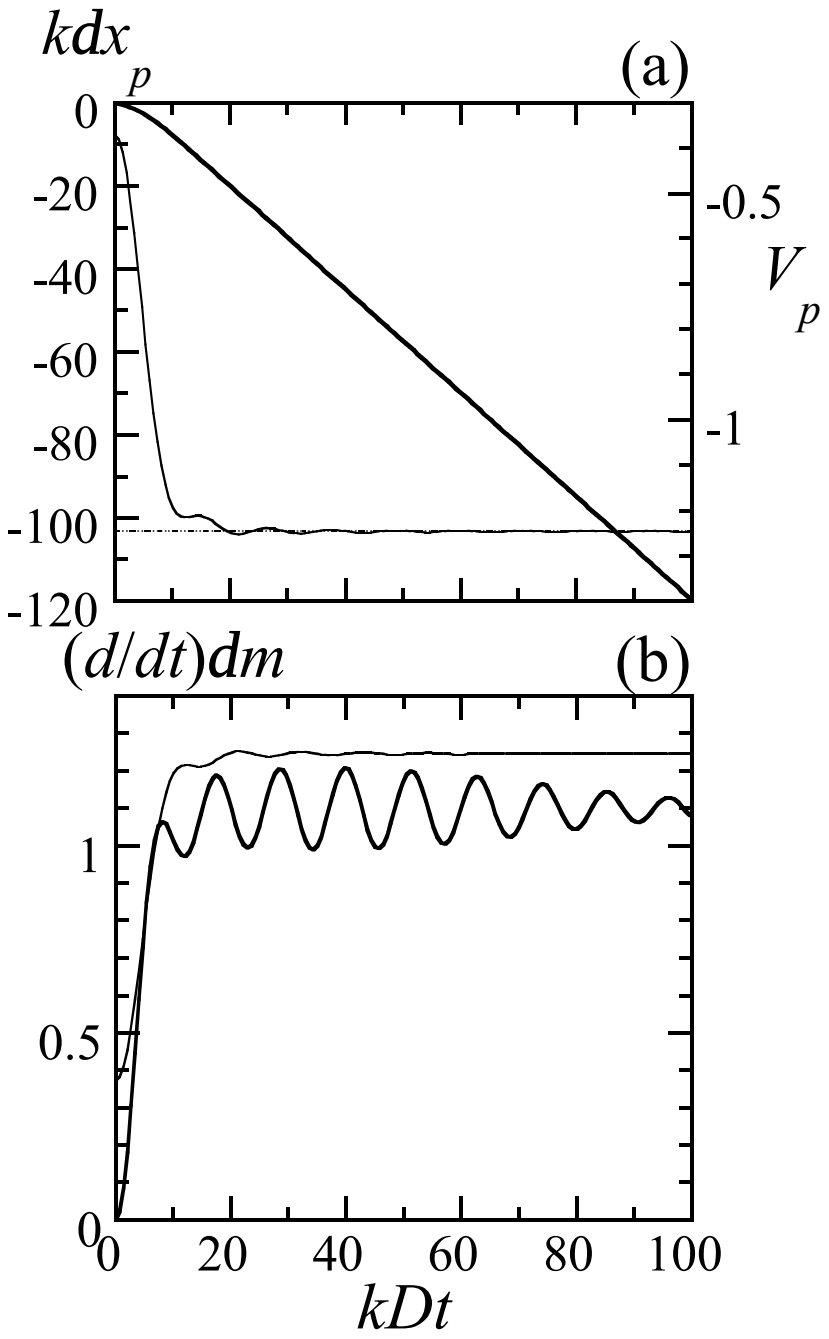

Figure 10. Normalized displacement amplitude of the piston surface kdx_p (thick), its time derivative V_p (thin), and the constant asymptotic value (88) (horizontal dashed line) (a); time derivative of areal mass modulation amplitude dm (thick) and contribution to it due to the surface ripple (thin line) (b) vs. normalized time kDt for the "stripes" pre-shock density perturbation, $g = 5/3$, $M_1 = 10$, free surface boundary conditions at the piston.

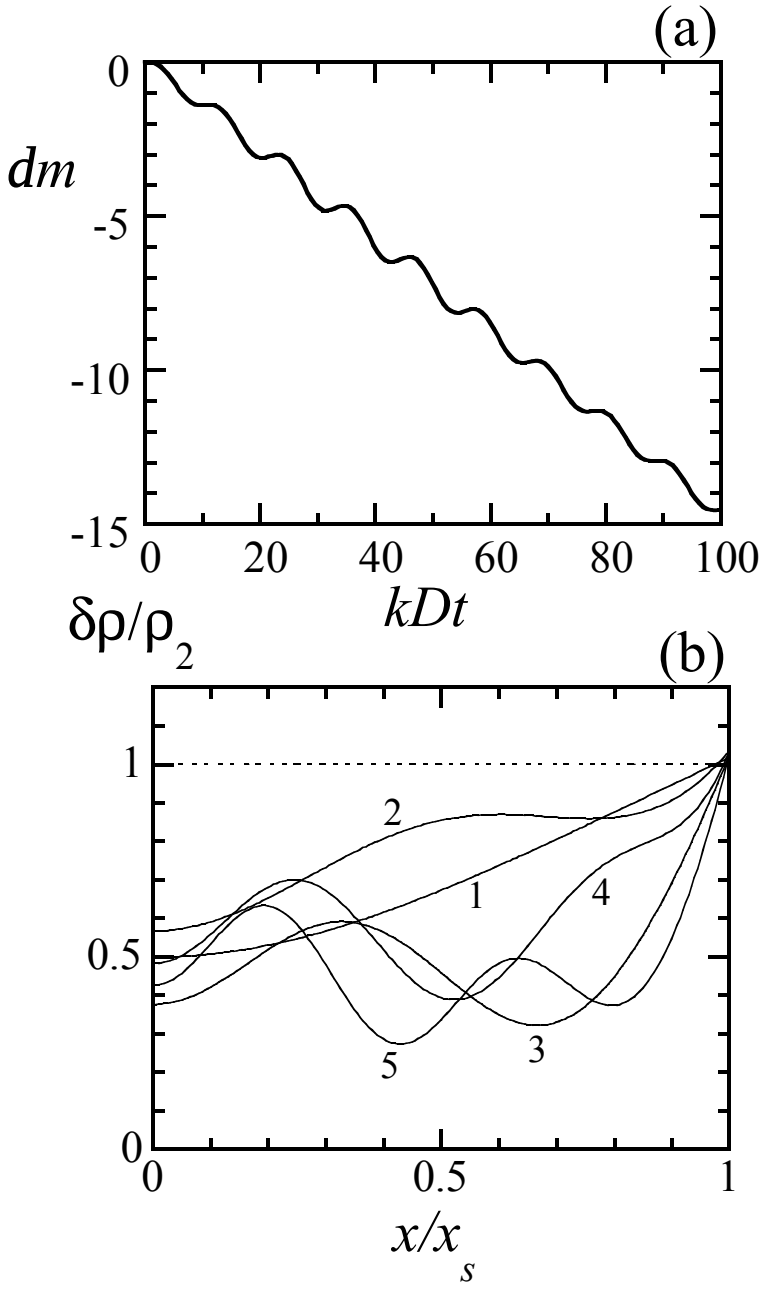

Figure 11. (a) Normalized areal mass modulation amplitude vs. normalized time kDt for the "stripes" pre-shock density perturbation, $g = 5/3$, $M_1 = 10$, rigid piston. (b) Relative post-shock density modulation amplitude profiles $\tilde{r} = dr / r_2$ shown at the times when the shock wave traveled 1, 2, 3, 4 and 5 lateral perturbation wavelengths (solid lines). Dotted horizontal line indicates the pre-shock relative density perturbation amplitude.

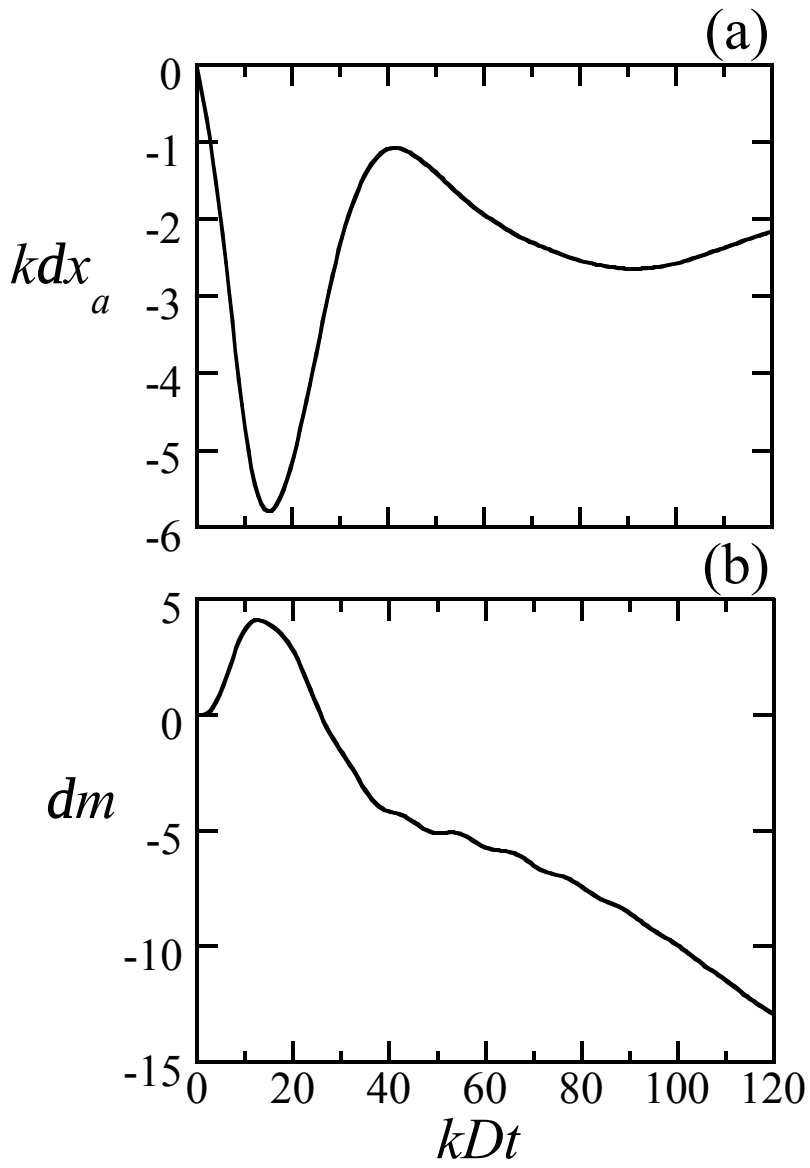

Figure 12. Normalized displacement of the ablation front kdx_a (a) and areal mass modulation amplitude dm (b) vs. normalized time kDt for a "stripes" density perturbation $g = 5/3$, $M_1 = 10$, and an ablation front with $r_D = 0.0625$, $M_a = 0.05$ acting as a piston.

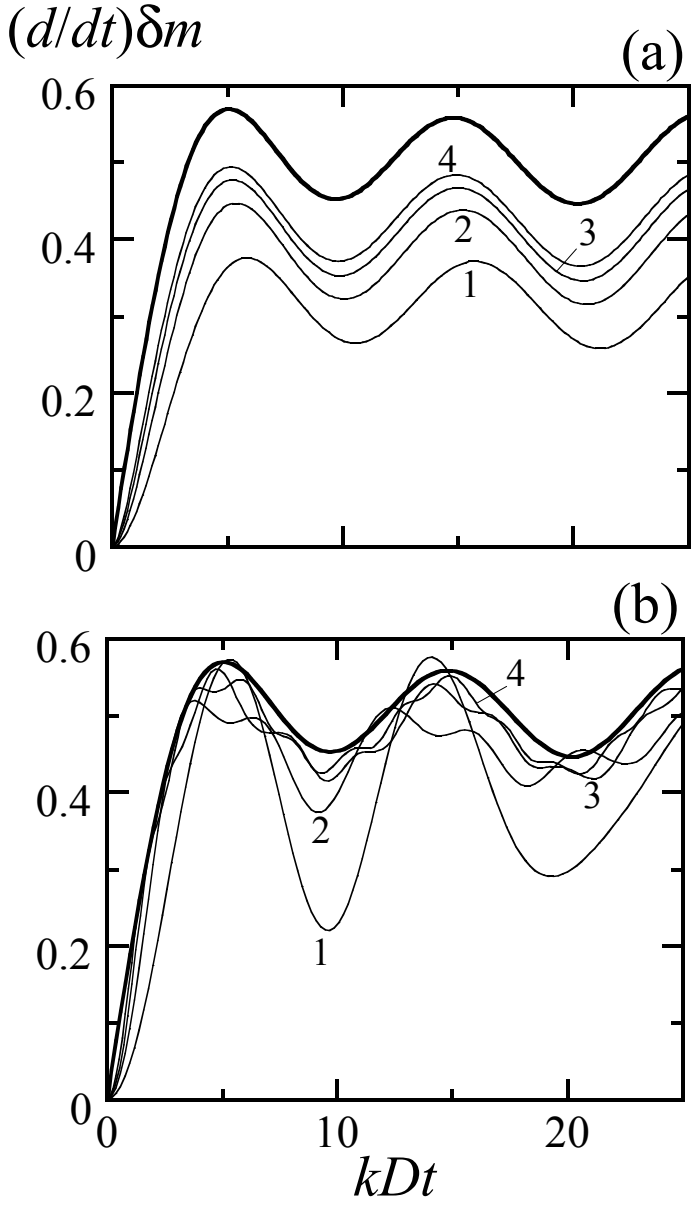

Figure 13. Normalized time derivatives of the areal mass modulation amplitude dm for surface ripples (thick lines), exponential (a) and Bessel-function (b) localized density perturbations in the target (thin lines, labeled by the value of the parameter q/k) vs. normalized time kDt for $g = 5/3$, $M_1 = 10$.

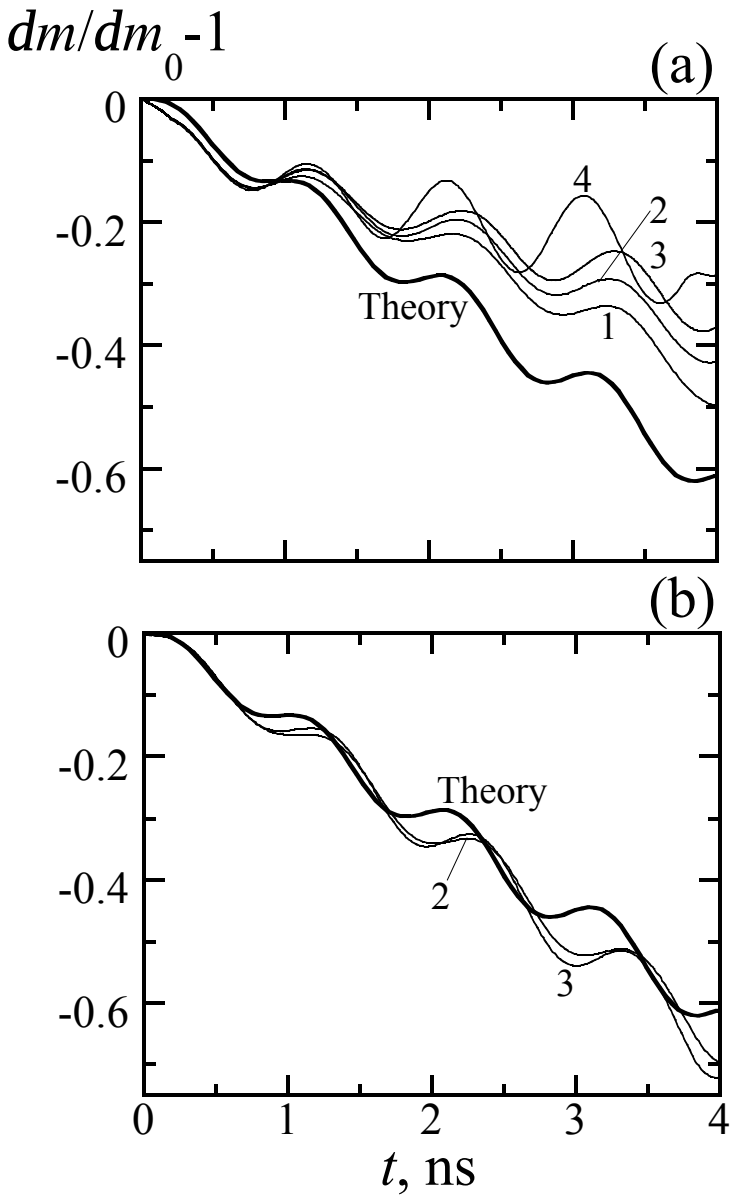

Figure 14. Theoretical and simulated time histories of normalized areal mass modulation amplitude for the "stripes" case: $g = 5/3$, $M_1 = 10$, lateral perturbation wavelength $l = 30$ μm, rigid piston velocity $V_p = 4\times10^6$ cm/s. Lines 1 through 4 correspond to the values of the small-amplitude parameter $e = 5\times10^{-4}$, 2.5×10^{-3}, 10^{-2} and 5×10^{-2}, respectively. (a) Simulation done with a constant time step; (b) time step initially reduced.

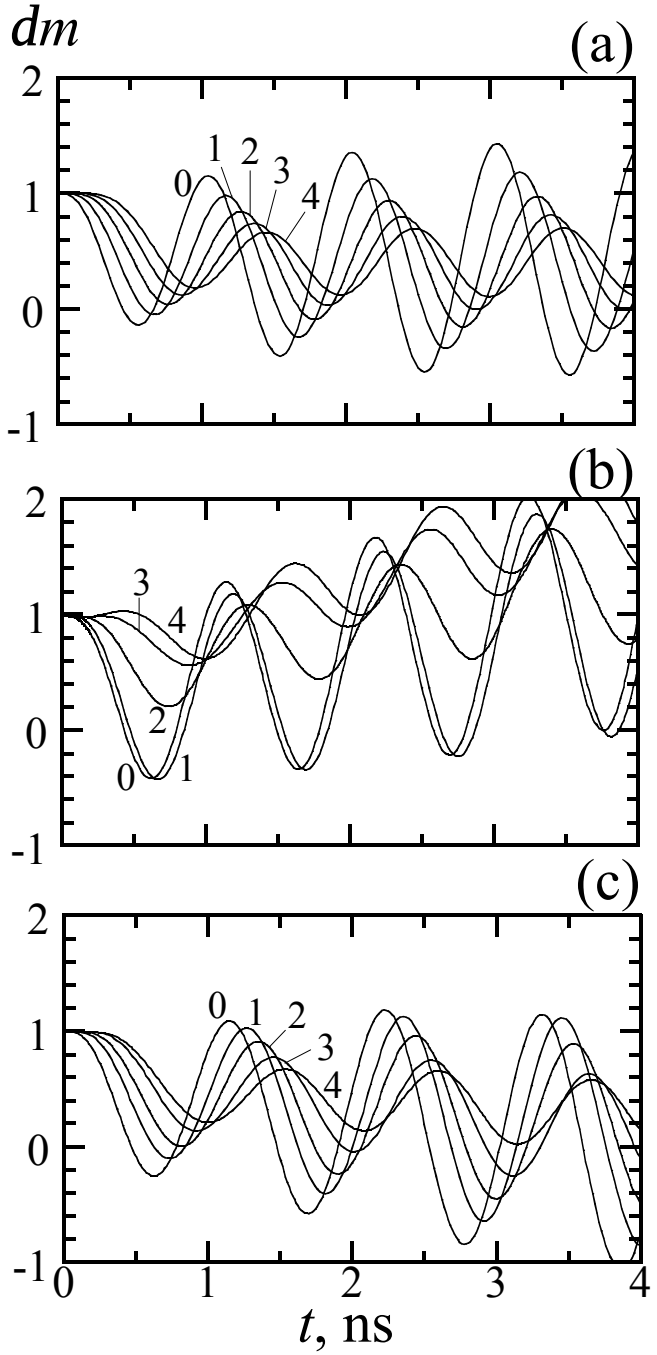

Figure 15. Normalized areal mass modulation amplitude dm vs. time for density modulation profiles (97) localized near the surface: $g = 5/3$, $M_1 = 10$, lateral perturbation wavelength $l = 2p/q = 30$ μm, rigid piston velocity $V_p = 4\times10^6$ cm/s; in the simulations, effective ripple amplitude $dx_0 = 0.1$ μm: (a) theory, (b) simulation with constant time step, (c) simulations with initially reduced time step. Lines 0 through 4 are indexed by the value of the parameter n in (97).